JOURNAL OF GEOPHYSICAL RESEARCH, VOL. 98, NO. C8, PAGES 14,401–14,421, AUGUST 15, 1993
10.1029/93JC00658

Observations of Vertical Currents and Convection in the Central Greenland Sea During the Winter of 1988–1989

FRIEDRICH SCHOTT, MARTIN VISBECK, AND JÜRGEN FISCHER

Institut für Meereskunde an der Universität Kiel, Kiel, Germany

During the winter of 1988–1989 five acoustic Doppler current profilers (ADCPs) were moored in the central Greenland Sea to measure vertical currents that might occur in conjunction with deep mixing and convection. Two ADCPs were looking up from about 300 m and combined with thermistor strings in the depth range 60–260 m, two were looking downward from 200 m, and one was looking upward from 1400 m. First maxima of vertical velocity variance occurred at two events of strong cold winds in October and November when cooling and turbulence in the shallow mixed layer generated internal waves in the thermocline. Beginning in late November the marginal ice zone expanded eastward over the central Greenland Sea, reaching its maximum extent in late December. In mid-January a bay of ice-free water opened over the central Greenland Sea, leaving a wedge of ice, the "is odden," curled around it along the axis of the Jan Mayen Current and then northeastward and existing well into April 1989. Below the ice a mixed layer at freezing temperatures developed that increased in thickness from 60 to 120 m during the period of ice cover, corresponding to an average heat loss of about 40 W m^{-2}. Through brine rejection, mixed-layer salinity increased steadily, reducing stability to underlying weakly stratified layers (Roach et al., 1993). During the ice cover period, vertical currents were at a minimum. After the opening of the ice-free bay, successive mixed-layer deepening to >350 m occurred in conjunction with cooling events around February 1 and 15, accompanied by strong small-scale vertical velocity variations. Upward mixing of more saline waters of Atlantic origin during this phase reduced the stability further, generating a pool of homogeneous water of >50 km horizontal extent in the central Greenland Sea, preconditioned for subsequent convection to greater depths. Individual convection events were observed during March 6–16, associated with downward velocities at the 1400-m level of about 3 cm s^{-1}. One event was identified as a plume of about 300-m horizontal scale, in agreement with recently advanced scaling arguments and model results, and with earlier similar observations in the Gulf of Lions, western Mediterranean. The deep convection occurred in the center of the ice-free bay; hence brine rejection did not seem necessary for its generation. Plume temperatures at 1400 m were generally higher than that of the homogeneous surface pool, suggesting entrainment of surrounding warmer waters on the way down. Mean vertical velocity over a period of convection events was indistinguishable from zero, suggesting that plumes served as a mixing agent rather than causing mean downward transport of water masses. However, different from the surface pool that was governed by mixed-layer physics, the water between 400 and 1400 m was not horizontally homogenized in a large patch by the sporadic plumes. Overall, and compared to results from the Gulf of Lions, convection activity in the central Greenland Sea was weak and limited to intermediate depths in winter 1988–1989.

1. INTRODUCTION

From water mass properties, it is known that the deep water of the Greenland Sea basin must be in direct exchange with the surface. Bottom water salinities and temperatures are lower than in the neighboring deep basins [*Aagaard et al.*, 1985]. Maximum deep values in tritium [*Smethie et al.*, 1986] and freon distributions [*Rhein*, 1991] can only be caused by convection and deep mixing of Greenland Sea surface waters. Yet, ongoing deep convection has never been observed in the Greenland Sea, and homogeneous water columns as its result are only sparsely documented. In a winter 1982 survey of the R/V *Hudson*, no evidence of convection was found at all [*Clarke et al.*, 1990]. In February 1988, *Rudels et al.* [1989] observed homogeneous water mass properties at only one position, and only down to 1300 m. During the Greenland Sea Project in winter 1988–1989 [*GSP Group*, 1990], extensive surveys were carried out across the Greenland Sea in November and again in February/March. No evidence for deep mixing was found during the *Meteor* cruise in early winter, but during the February/March cruise of the R/V *Valdivia*, homogeneity down to 1500 m was detected at one station [*Rhein*, 1991].

Preferred sites for deep convection as observed, e.g., in the western Mediterranean [*MEDOC Group*, 1970] and the Labrador Sea [*Lazier*, 1973; *Clarke and Gascard*, 1983], are regimes with cyclonic rotation over weakly stratified deep layers. The central Greenland Sea is an area which shows pronounced isopycnal doming [e.g., *Dietrich*, 1969; *Quadfasel and Meincke*, 1987; *Koltermann and Lüthje*, 1989], caused by the cyclonic circulation around it (Figure 1*a*). Large-scale cyclonic circulation conditions are prescribed by the currents around the region, i.e., the Norwegian Atlantic Current (NAC) and West Spitzbergen Current (WSC) flowing northward in the east, the East Greenland Current (EGC) flowing southward in the west, and the Jan Mayen Current (JMC) branching off to the east from the EGC along 72°N. The surface mixed-layer depth in the center of the isopycnal dome of such a regime is at a minimum, and hence this is the spot where stability against the deeper layers can be overcome first by density increases caused by surface cooling, evaporation, or possibly brine rejection related to ice formation. The specific location of the Greenland Sea cyclonic gyre may also have to do with bottom trapping of the wind-driven circulation [*Legutke*,

Paper number 93JC00658.
0148-0227/93/93JC-00658$05.00

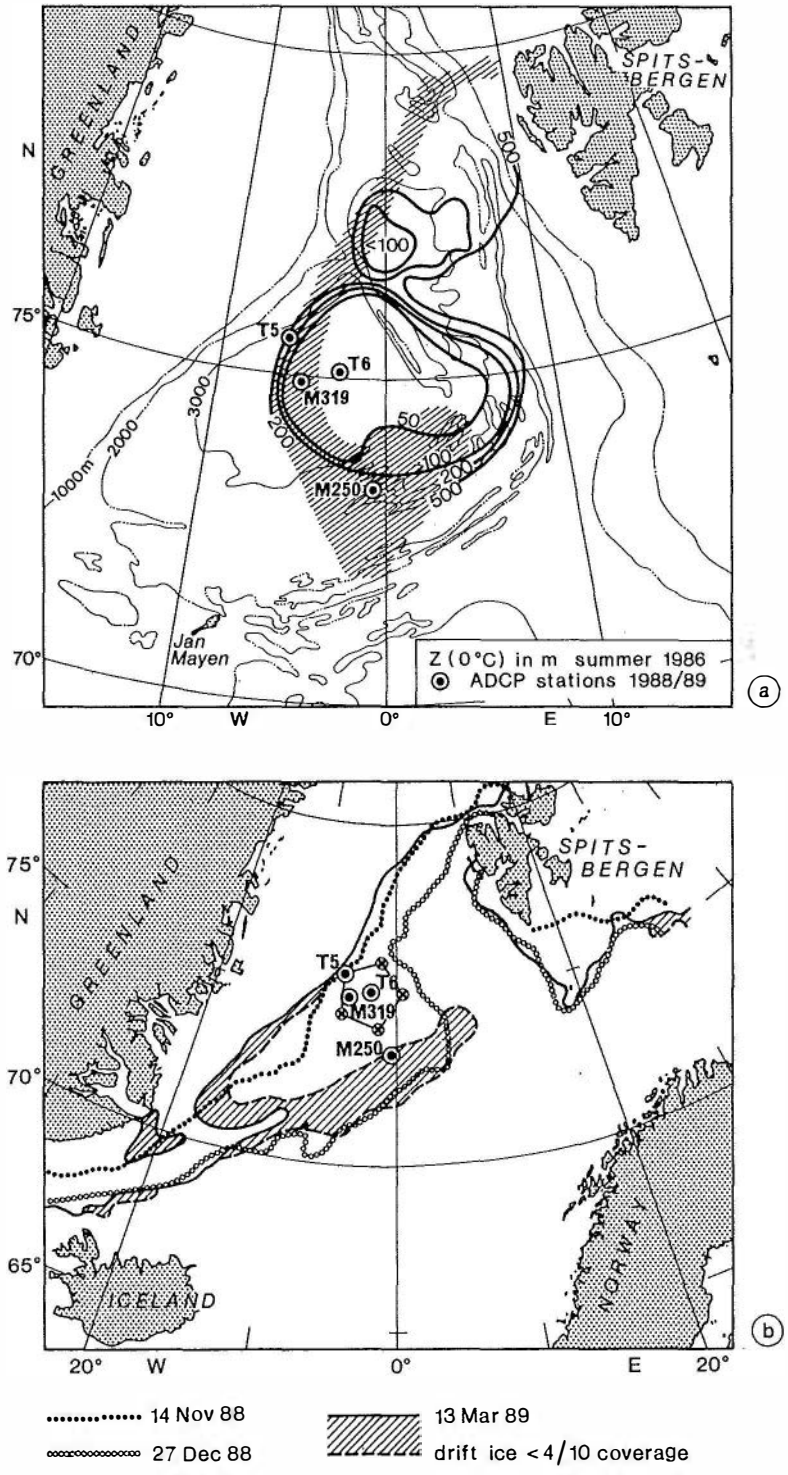

Fig. 1. (*a*) Positions of ADCP measurements. Superimposed is depth of 0°C isotherm for summer 1986 and climatological mean position (shaded) of Marginal Ice Zone in March [from *Quadfasel and Meincke*, 1987]. T5 and T6 were moorings of Scripps/WHOI tomography array, into which our ADCPs were incorporated. (*b*) Locations of Marginal Ice Zone during winter 1988–1989 and of ADCP moorings. The wedge (is odden) penetrating northeastward in March 1989 is for ice concentrations between 0.4 and 0.7.

1991], Sometimes a second, smaller cyclonic regime exists to the north, in the Boreas basin (Figure 1*a*). Stability at the low temperatures of the central Greenland Sea is heavily affected by small changes in salinity (at −1°C, a 0.02 psu salinity change has a density effect equivalent to a 0.5°C temperature change).

The exact cause of deep convection in the central Greenland Sea could not be determined from the few observations. Cooling alone is not the cause, because the early winter mixed-layer salinity at freezing temperature will still be stably stratified.

Hence, salinity increase associated with ice formation is a

prime candidate for initiating deep convection in the Greenland Sea. *Rudels* [1990] proposed a mechanism for plume formation and subsequent deep convection out of brine rejection, but existing observational evidence has not been detailed enough to test this hypothesis. Another possibility could be ice-edge upwelling [*Häkkinen*, 1987; *Guest and Davidson*, 1991]: for winds blowing about parallel to the ice edge with the ice to their right, the higher drag coefficient over the ice causes an Ekman divergence at the ice edge. The consequence could be upwelling of warmer and saltier water, which when cooled to the freezing point, would have the necessary density to overcome the stability of the dome. The lack of deep mixed-layer observations in the Greenland Sea inspired explanations based on subsurface processes, by cabeling [*Carmack and Aagaard*, 1973] or by double diffusion, acting on the Atlantic water being advected into the area from the southeast [*McDougall*, 1983].

In the context of the Greenland Sea Project (GSP), direct measurements of the three-dimensional currents were carried out with moored acoustic Doppler current profilers (ADCPs) to detect vertical currents associated with convection if they occurred. In a previous study in the convection regime of the Medoc area, Golfe du Lion, such devices had already been used to document vertical currents during strong convection events caused by the cold and dry Mistral winds of the region [*Schott and Leaman*, 1991] (hereinafter referred to as SL91). These measurements, carried out within a patch of homogeneous water formed prior to the ADCP deployment, showed that with the onset of surface cooling, downward velocity events of about 5 cm s^{-1} vertical velocity and periods of less than 2 hours occurred. In between these downward events, weaker upward motion occurred, but the mean vertical velocity over the 1-week period of surface cooling was downward, at about 1 cm s^{-1} in the 300- to 500-m depth range at the mooring site. From the time scale of the events, less than 2 hours, and the advective speed, less than 20 cm s^{-1}, a horizontal scale of only O(1 km) was estimated for these events by SL91. Whether the horizontal circulation associated with these downward events had a preferred sense of rotation could not be satisfactorily established from these single mooring data.

Recent numerical modeling work [*Brugge et al.*, 1991; *Jones and Marshall*, 1993] and laboratory experiments (T. Maxworthy and S. Narimousa, personal communication, 1991) showed that the large-scale surface buoyancy flux may indeed create small-scale cells ("plumes") of downward motion. While at the beginning of the forcing these cells are three-dimensional, they get organized into geostrophic vortices as time becomes comparable with the inertial period. Their horizontal scale for neutral stratification is only dependent on two external parameters, buoyancy flux and Coriolis parameter, and is typically <1 km [*Jones and Marshall*, 1993].

Since for the Greenland Sea so little evidence for deep convection had been produced earlier, the five available ADCPs were distributed on a larger scale (Figure 1) to obtain some statistics on the occurrence of deep mixing and the associated vertical velocity variations rather than trying to cover the O(1 km) event scale with several instruments simultaneously. Two of the stations, T5 and T6 (Figure 1*a*), were part of the tomography array of Scripps/Woods Hole Oceanographic Institute (WHOI) [*Worcester et al.*, 1991; *Roach et al.*, 1993; GSP tomography group, personal communication, 1992] into which our instruments were incorporated.

This paper, after a description of the measurement setup and a discussion of data retrieval and accuracy of the different measurement systems, summarizes the general meteorological, hydrographic, and ice conditions around the observation sites; then presents the ADCP measurement results and subsequently focuses on time periods of enhanced vertical velocity activity. As will be shown, throughout most of the winter, evidence for homogenization is restricted to the upper few hundred meters. In the first half of March, however, at a time when homogeneous profiles down to 1500 m have been observed in the central Greenland Sea [*GSP*, 1990; *Rhein*, 1991], individual short-term events of significant downward motion are observed down to the 1400-m ADCP level. As will further be shown, this sporadic convection activity is not occurring when the ice edge is in the immediate vicinity of the measurement sites but rather when stations are located in the center of the ice-free area or "nordbukta" [*Vinje*, 1977] between the marginal ice zone in the west and the tongue of ice ("is odden") curling around it from the south and east.

2. MOORED ARRAY AND DATA QUALITY

ADCP Array Configuration

The ADCPs, operating at 153.6 kHz, were similar to those used in the previous convection experiment of SL91, except that the data storage capacity was increased by using 60 Mbyte tape cassette recorders rather than the earlier version, which had been limited to 2 Mbyte and would not have allowed sufficient temporal resolution over the entire winter period. Two ADCP moorings (250 and 319, Figure 1) were deployed carrying upward looking ADCPs at 362 m and 342 m, respectively. Mooring 319 was located at 74.9°N, 5.0°W, and mooring 250 to the southeast at 73.3°N, 1.0°W, in a region of more stable stratification at the rim of the cyclonic dome (Figure 1*a*). Originally, this latter station had been planned for deployment at 73°N, 8°W, but due to ice conditions at deployment time and ship time limitation it had to be deployed that much to the east. Above the ADCPs in moorings 250 and 319, and carried by hard-foam floats at 78 m, and 60 m, respectively, 200-m-long thermistor strings (type Aanderaa) were mounted to record the temperature stratification at depth increments of 20 m (Figure 2*a*). Earlier tests with 150-kHz ADCPs had shown [*Schott*, 1988] that neither the floats nor the thermistor string should have an adverse effect on the ADCP echo amplitude or Doppler velocity profiles. Directly below the ADCPs in moorings 319 and 250, an Aanderaa rotor current meter (ACM) was positioned for intercomparison, and two and three, respectively, more ACMs were recording currents at deeper levels (Figure 2*a*).

The other three ADCPs were incorporated into the acoustic tomography array of the WHOI/Scripp's Institute of Oceanography (SIO) group. Since these carried large tomographic sources at about 100-m depth (Figure 2*b*), which might cause reflections of vertically traveling side-lobe signals and thus biases of the main beam backscatter returns, ADCPs could not be applied in the upward looking mode in the upper 350 m of these moorings. Instead ADCPs were placed in the downward looking mode at 140-m depth in

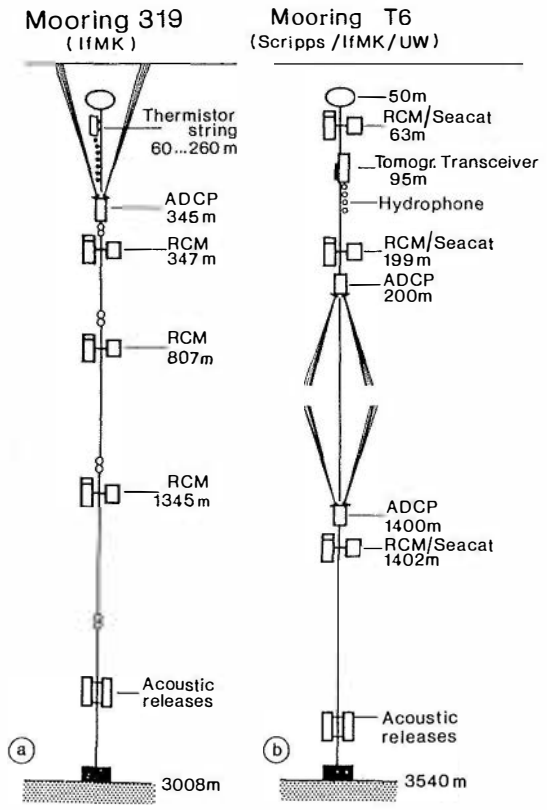

Fig. 2. (*a*) Institut für Meereskunde an der Universität Kiel (IfM Kiel) mooring M319 with upward looking ADCP at 345 m combined with thermistor string between 60 and 260 m, and with three rotor current meters below. (*b*) Scripps/WHOI tomography mooring T6 with ADCPs at 200 m (looking downward) and 1400 m (looking upward) of IfM Kiel. Also included in that mooring were rotor current meters and "Seacat" temperature-conductivity recorders at three depths by University of Washington [see *Roach et al.*, 1993].

moorings T5 and 200 m in T6, respectively, where they were facing unobstructed depth ranges (Figure 2*b*). T6 was located 60 km to the east of 319, and T5 about 75 km to its northwest (Figure 1). To detect deep convection if it occurred, another ADCP was positioned at 1400-m depth in mooring T6, looking upward (Figure 2*b*). The upper ADCP on T6 will be called T6U, the lower one T6L in the following.

All ADCPs had 20° beam angle configuration. Using two-axis tilt sensor and fluxgate compass, the beam Doppler velocities for each transmitted signal (ping) were transformed into Earth coordinates by an internal processor. The Doppler data from 125 pings, which were transmitted at 1-s intervals, were vector averaged into an ensemble and recorded on tape cassette. The time interval between the 125-s ensembles was 30 min in moorings 250, 319, and T5, and 60 min in mooring T6. The reason for the longer time interval between ensembles at T6 was to avoid interference with the acoustic tomography transmissions and with each other. Vertical bin length was 8.6 m in moorings 250, 319, and T5, and 17.2 m in T6.

According to the manufacturer [*RD Instruments*, 1989], these parameter settings yield a nominal accuracy of the horizontal ensemble velocity component of 1.7 cm s^{-1} for instruments in moorings 250, 319, and T5, and 0.9 cm s^{-1} for those in T6. Due to the 20° beam configuration, the nominal accuracy of the vertical velocity is significantly better with 0.6 cm s^{-1} for moorings 250, 319, and T5, and 0.3 cm s^{-1} for those in T6.

The number of bins recorded was 64 in moorings 250 and 319 in order to always have the surface in the range of the ADCP, even in the unlikely case of fairly large depth excursions. In ADCPs T5, 65 bins were stored, and in T6U and T6L, 32 bins (of double length).

The overdetermination of four available beams for three coordinates allows the calculation of a consistent velocity, called error velocity. It is the difference of vertical velocities calculated from the two orthogonal beam pairs and should be of the order of the nominal vertical velocity accuracy. If it is not, it suggests either poor data quality or significant velocity shear within the spacing of the acoustic beams. At 200-m range the beam spacing for the 20° beam inclination amounts to 150 m. The error velocity thus can serve as an additional indicator for the horizontal scale of convection events.

ADCP Performance and Profile Evaluation

Comparison of ADCP currents with Aanderaa rotor current meters (ACMs) revealed large deviations in ADCP current directions, although the ADCP compasses had been recently calibrated by the manufacturer. These deviations were dominantly in the first harmonic, i.e., of one cycle per 360° with amplitudes ranging from 14° to 37° for the different instruments. It then turned out that the calibration of the fluxgate compass carried out by the manufacturer in San Diego, California, was site dependent, being a function of strength and vertical inclination of the Earth's magnetic field. Since the residual variance of the direction difference between ADCP and ACM, after correction of the ADCP directions, still remained between 5° and 10° for the ADCPs on stations 250, 319, and T6, with no comparison possible at T5, the quality of the horizontal currents has to be considered degraded.

There was also a significant difference in speeds recorded by ADCPs on stations 319 and 250 compared to those measured by ACMs directly below (Figure 2*a*): Aanderaa speeds were only about 70% of ADCP speeds. This was surprising, since the same ADCPs had given good speed comparisons with ACMs in similar subsequent deployments in the Mediterranean and Atlantic. The special distinction to those later comparisons is the low temperature (of about −1°C), and it is not clear at this point which type of instrument was the culprit.

Instrument pitch and roll sensors showed small ensemble means and standard deviations, indicating that instrument behavior should not cause biases in the decomposition of beam Dopplers into vertical and horizontal components.

The deployment mean echo amplitude profiles of the five ADCPs (Figure 3*a*) show similar decay rates, as expected from sound propagation theory (spherical spreading and attenuation). For upward looking ADCPs on stations 250 and 319 the maxima indicate surface backscatter, which will be used in the following to determine ice cover. The percentage of good data on the right-hand side of the graph indicates the data with signal-to-noise (S/N) ratio exceeding 3 dB (the default value) in all four beams simultaneously. This would suggest about 300-m range, but caution has to be applied: at low S/N, the bin to bin tracking can be biased, resulting in biased current shears [*Chereskin et al.*, 1989]. Hence the

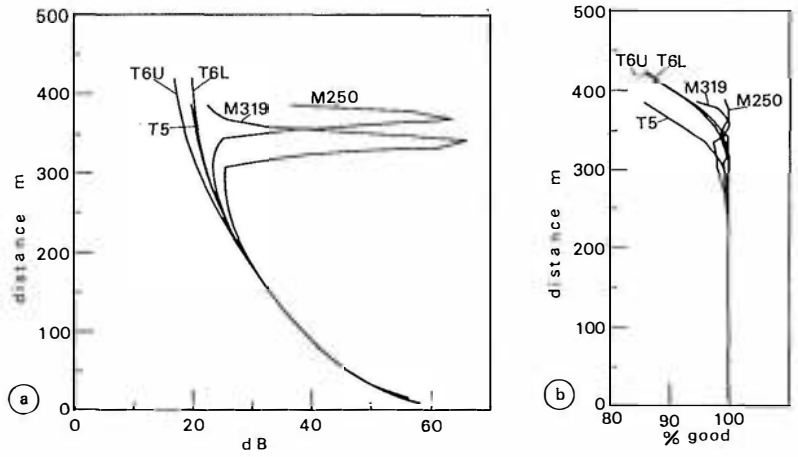

Fig. 3. (*a*) Record length mean echo amplitude profiles (decibels) for the five ADCPs and (*b*) percentage of good data. The peaks for M250 and M319 are caused by surface echo.

cutoff of good data may actually occur at a lesser distance from the transducer, but since we have no precise way of determining this range, we show the data over the 300-m range.

Moored Rotor Current and Temperature Data

Rotor current meters used on stations 250 and 319 were all of type Aanderaa RCM5, and the time interval of the observations was 1 hour. At periods of low currents (typically <3 cm s^{-1}) the rotors of these instruments stalled, and an artificial velocity of 2 cm s^{-1} was applied to visualize the recorded direction changes. With regard to quality of the speed measurements, the significantly lower values compared to those measured by ADCPs were already mentioned.

Temperature records from three types of instruments were used to monitor the changes of the thermal stratification within the water column: Aanderaa thermistor strings in the near-surface range with a thermistor spacing of 20 m at stations 319 and 250, temperature sensors on Aanderaa rotor current meters in intermediate and deeper layers, and ADCP temperature sensors at stations T5 and T6. The ADCP temperature sensors at stations 250 and 319 returned doubtful data and will not be used in the following.

The time resolution for the thermistor string data was 2 hours, and for all other instruments it was 1 hour. Unfortunately, due to a technical problem of the thermistor string recorder on station 319 the time of that record is only determined to within 2 hours, which does not permit combining the recorded temperature fluctuations with the ADCP vertical velocity fluctuations for calculation of heat flux carried by the short-period events.

All Aanderaa thermistors were set to "low" and, if available, "arctic" range, yielding a resolution of 0.023°C and 0.008°C, respectively. The thermistor string sensors were factory calibrated before deployment, and subsequent comparison with a conductivity, temperature, and depth (CTD) station on March 1 in the vicinity of mooring 319 was within ±0.02°C for record averages over the duration of the CTD cast, when all sensors were in the deep mixed layer, and the standard deviation of the sensors during the period of the cast was ±0.03°C. Although five stations were available during the GSP fairly close to mooring 319, only the late winter station could be used for calibration purposes; the variance for the other CTD casts in fall and late spring was too large to achieve stable means. The ACM temperature sensors needed offset corrections of the order of 0.1°C, since they had not been calibrated prior to deployment, and the standard deviation during the March 1 CTD station was ±0.04 for the 347-m-deep sensor and ±0.006 for 1345-m depth. For the ADCP temperature sensors (station T6) two casts from March 9 were used and yielded offset corrections of 0.25°C for the lower ADCP (T6L) and 0.03°C for the upper instrument (T6U). No in situ calibration could be carried out at station 250 due to the lack of late winter CTD stations. No trend corrections were applied, and the resulting accuracy is expected to be 0.05°C for the calibrated temperatures.

3. Meteorological, Ice, and Hydrographic Conditions

Meteorological Conditions

The mean winter wind conditions are characterized by northerly wind directions caused by the Greenland pressure high against lower pressures over the ocean. Direct wind observations from the central Greenland Sea are only available during November/December 1988 when the R/V *Meteor* was in the area, and for February/March 1989 from a *Valdivia* cruise.

Wind stress fields and heat flux components were obtained from the European Center for Medium-Range Weather Forecasts (ECMWF) model at 6-hour time intervals and approximately 1° latitude × 1° longitude resolution. Since the research vessel observations were most likely included in the ECMWF model assimilation, they could not be used for independent comparison; a regression for a sample of 233 different ship observations from the Greenland Sea during the observational period with ECMWF winds resulted in a correlation coefficient of 0.96 for the directions and 0.65 for the stress values. An independent evaluation of at least the wind directions could, however, be carried out using the surface backscatter from the upward looking ADCPs, because the surface bin Doppler shift has been found previously to correlate very well with wind direction [*Schott*, 1989]. The result for our ADCP stations was that the

ECMWF wind directions compare surprisingly well (with a correlation coefficient of 0.95 for station 250 and 0.98 for station 319 for the September–October period) with the ADCP Doppler directions [*Mirbach*, 1991], providing some confidence in the ECMWF model product; despite the very sparse data support, it is based on in the Nordic Seas. The surface Doppler signal can, however, not be used for wind speed determination; it is either caused by the Bragg scattering effect of the small O(1 cm) ripples modulated by the longer surface waves or by near-surface bubble returns from the wave zone. Instead, the magnitude of the return energy from the surface (echoamplitude) has been shown to be positively correlated with wind speed in a semilogarithmic relation [*Schott*, 1989], but error bars on the regression coefficients are generally large and the echoamplitude is therefore not of much help in determining wind speed on an event time scale or assessing quality of ECMWF wind stresses.

Monthly mean ECMWF stress fields from over the central Greenland Sea for the winter months show generally southward and slightly westward directions and large decorrelation scale. The ECMWF stress is supposed to have an ice stress condition included (K. Arpe, personal communication, 1990), but due to the large decorrelation scale, one does not detect appreciable effects in the ECMWF wind stress fields over the known position of the Marginal Ice Zone (MIZ) in late winter. Hence it will be sufficient for the subsequent discussion to inspect just one time series of the ECMWF model output for wind stress from the central area.

The total heat flux of the ECMWF model from the central Greenland Sea shows fluctuations between 100 and 500 W m^{-2} heat loss during the winter months with a mean of 248 W m^{-2} for the November 1 to March 1 period. The component contributing the most was the sensible heat flux at 99 W m^{-2}, while mean evaporative heat flux was 72 W m^{-2}. Maximum heat flux occurs in winter at times of winds from the west or north that advect cold and dry air from over the ice toward the free water. Evaporation minus precipitation over the November to February period amounted to 0.2 m. Compared to the large scale of the stress fields, the ECMWF heat fluxes do show areas of significant horizontal gradients in the observational region during the period of partial ice cover. Mostly, though, the gradient zone stays east of the stations during late January to mid-March, and fluctuations are quite similar at positions 319, T5, and T6, which are of interest in the following. Heat fluxes calculated from shipboard meteorological observations of the R/V *Valdivia* for a few days in February and March when the ship was in the central Greenland Sea yielded reasonable comparisons with the ECMWF heat fluxes. Nevertheless, the ECMWF data can only serve as a rough indicator of what occurs at an individual station in the region.

An analysis of surface air pressure maps for special weather situations that might be favorable for deep convection was presented by *Guest and Davidson* [1991] and will also be used in the subsequent discussion of convection events.

Ice Conditions

During fall to early winter of 1988 the weekly ice maps of Norwegiske Meteorologiske Institut (NMI) show progressive eastward expansion of the MIZ east of Greenland, and by mid-November the first station of the array (T5) is passed by the MIZ. By late December, the ice-covered region bordered by a fairly well-defined MIZ has reached its farthest extent (Figure 1*b*). Insight into the more detailed evolution of the variable ice conditions during the later part of the season can be gained from special sensor microwave imager (SSM/I) ice concentrations, which are available at daily intervals at a resolution of 35 km [*Roach et al.*, 1993] (also, GSP tomography group, personal communication, 1992; L. Toudal, personal communication, 1992). In mid-January an area of ice-free water begins to form in the northern Greenland Sea [*Roach et al.*, 1993], spreading southward and reaching stations 319 and T6 during January 23–25. This phenomenon of a long wedge of ice curled around the central Greenland Sea is called "is odden," the ice-free area enclosed by it "nordbukta" [e.g., *Vinje*, 1977]. It is an annually recurring feature that shows up in the mean ice climatology (Figure 1*a*). It has strong interannual variability but also large changes in area coverage on time scales of only days to weeks. The is odden of 1989 continues to exist through March (Figure 1*b*) and vanishes in mid-April.

Additional information on the presence of ice over ADCP stations can be gained from the surface-reflected signals of upward looking ADCPs [e.g., *Belliveau et al.*, 1989]. A similar procedure was applied here for stations 319 and 250, which carried upward looking ADCPs at 342 m and 362 m, respectively, using the velocity variance and the strength of the surface backscatter signal, which both were low when ice was present. Combining satellite and moored ice data, we have constructed a time series of local ice coverage for each mooring site, distinguishing between three classes of ice concentrations: ice free (0–20%), sparsely ice covered (20–50%), and densely ice covered (>50%). Although there was some disagreement between the different ice data sets concerning the eastward extent of the MIZ in November, they showed an overall agreement regarding the general development of the ice cover during winter 1988–1989. The ice coverage is indicated in the pertinent figures by bar graphs. All methods provided only limited information on new ice formation, which could be relevant for the occurrence of convection in causing negative buoyancy flux due to brine rejection.

Hydrographic Conditions

The circulation in the Greenland Sea is characterized by pronounced doming: the 0°C isotherm rises from >500-m depth to <50-m depth over a distance of typically less than 100 km (Figure 1*a*). On the average, the center of this dome is located at about 75°–76°N and somewhat west of the Greenwich meridian [*Dietrich*, 1969; *Koltermann and Lüthje*, 1989]. The Arctic surface waters of the summer near-surface layer in the central Greenland Sea are characterized by salinities between 34.7 and 34.8 psu, and temperatures of 0–3°C. Stratification underneath the pycnocline is weak, with potential temperatures below 1500 m near −1.2°C and salinities near 34.895 psu [*Aagaard et al.*, 1985]. To the east, the Arctic domain is separated from the warmer, saltier waters of Atlantic origin by the Arctic front that in the Greenland Sea is located over the Mid-Atlantic Ridge, i.e., near 6°–8°E. To the west, it is separated from the colder, fresher polar waters of the East Greenland Current by the polar front.

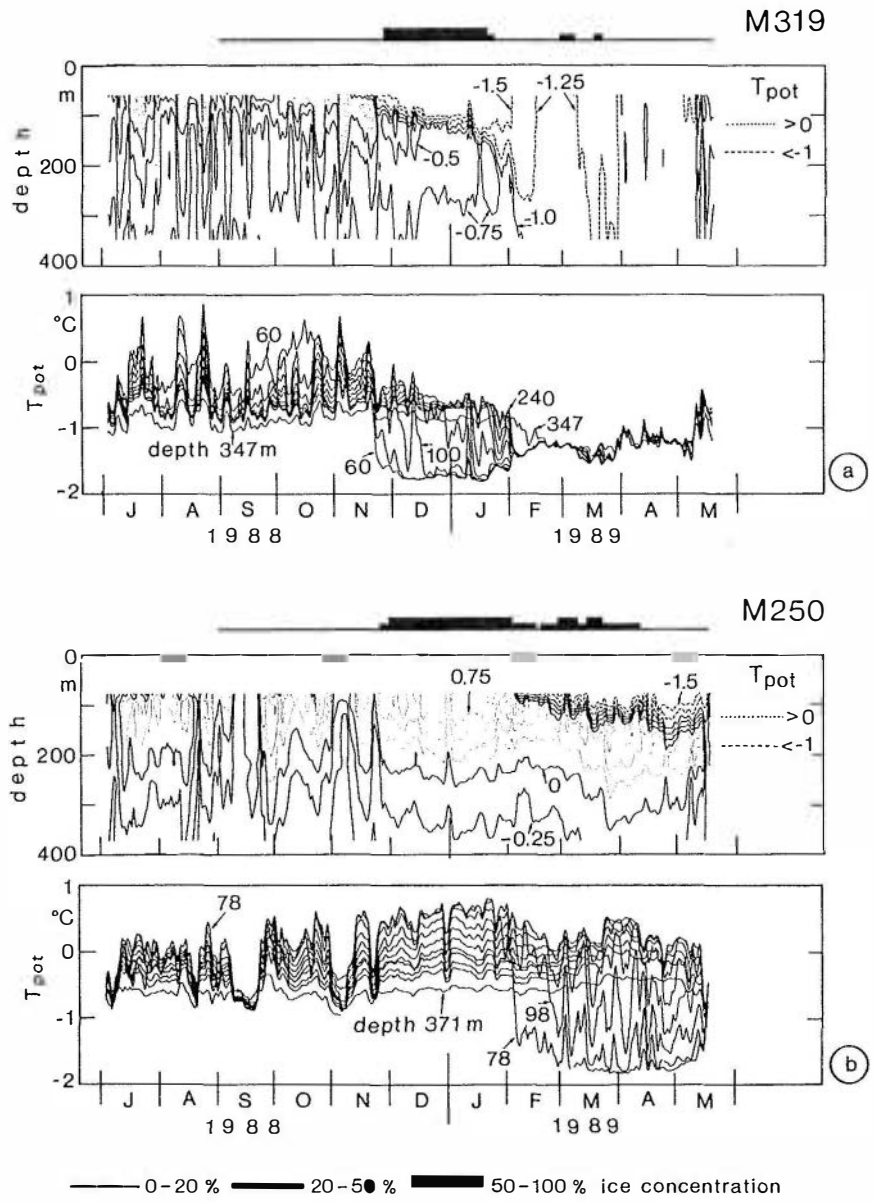

Fig. 4. (*a*) Time series of low-passed potential temperatures recorded by thermistor string on station 319 in 60- to 260-m depth range and by ACM at 347-m depth (bottom) and low-passed contour plot for 60–350 m (top). Ice concentration shown by bar graphs. (*b*) Same as Figure 4*a* but for station 250 and slightly different instrument depths. (*c*) Unfiltered potential temperatures in the 140- to 200-m depth range at stations 319, T5, and T6. Ice coverage indicated by bar graphs (see text for details). (*d*) Same as Figure 4*c* but for 1345- to 1437-m depth range at stations 250, 319, and T6.

Hydrographic station data of summer 1988 (J. Meincke, personal communication, 1991) showed the existence of the dome in roughly the same area as in 1986 (Figure 1*a*). Position T6 was well in its center, position 319 was still within the dome, position T5 at the western rim, i.e., in the zone affected by the polar front, and position 250 clearly at the southwestern stratified flank of the dome. A zonal hydrographic section by R/V *Valdivia* in February 1989 along 74°45′N showed the doming in existence below about 600 m in the temperature distribution, and centered between 5°W and 3°E [*van Aken et al.*, 1991].

The thermistor chain data of positions 319 (Figure 4*a*) and 250 (Figure 4*b*), augmented by ACM thermistors from deeper instruments show the stratification between 60 and 350 m and 78 and 400 m, respectively, over the course of the year, and document the drastic differences between both sites.

At position 319, temperature gradients during July to November were typically <1°C across the 60- to 260-m layer with in-phase variations of the order of several weeks. With the onset of ice coverage, as indicated by the bar graphs in Figure 4 for coverage of 20--50% and >50%, cooling to near-freezing temperatures and successive increase of mixed layer thickness under the ice occurred from 60 m in late November to 200 m in late January. This cooling corresponds to an average heat loss of about 40 W m^{-2} of the surface layer. As to be expected and shown by the Seacat records of *Roach et al.* [1993] from the central Greenland Sea, the salinity within the mixed layer increases during the period of ice cover, reducing stability and making the

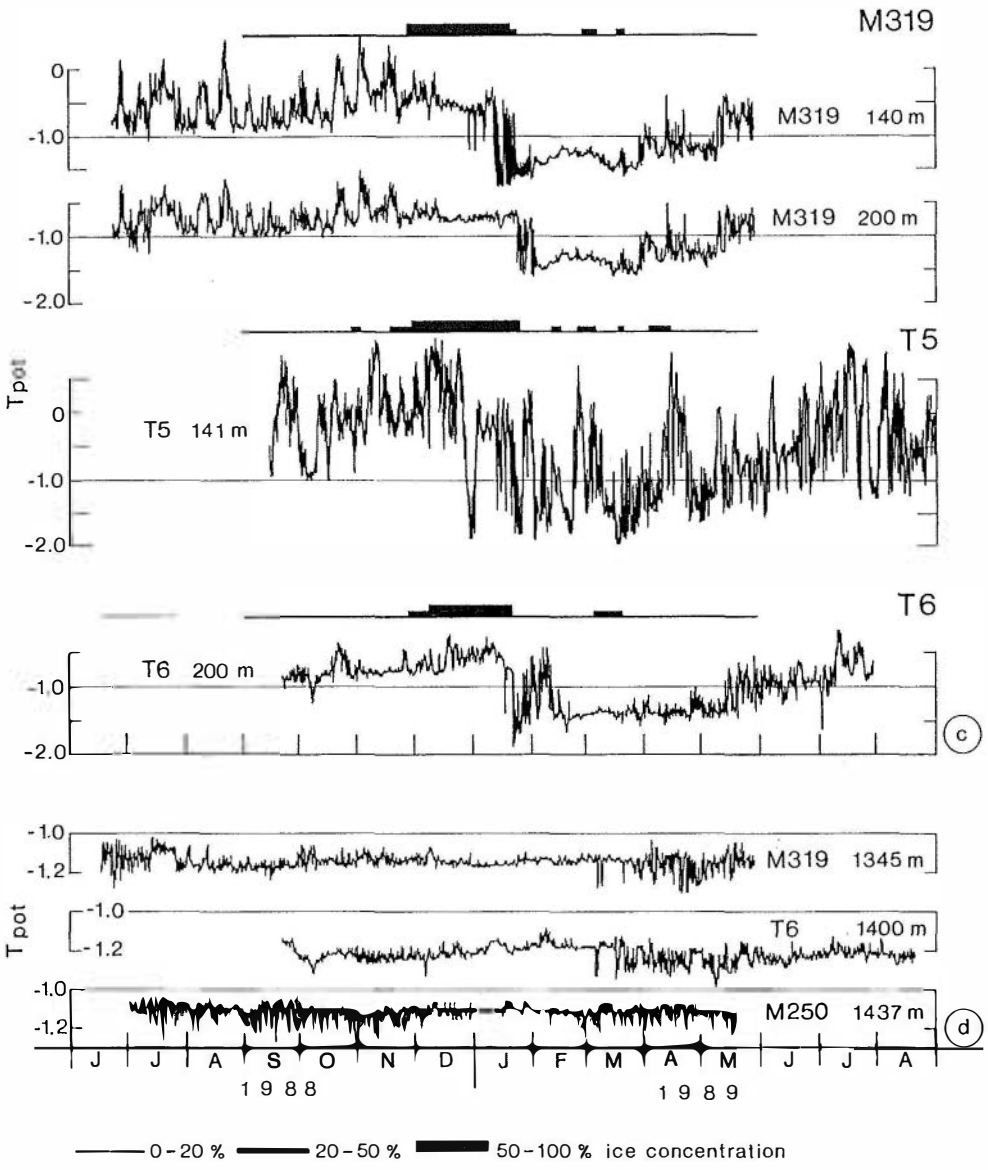

Fig. 4. (continued)

column vulnerable for deep mixing and convection once the ice is removed.

The most drastic change of near-surface stratification in the central Greenland Sea occurred during late January to mid-February when the mixed layer successively deepened to >350 m (Figures 4*a* and 4*c*), where the further vertical extent of homogenization could not be determined due to lack of temperature sensors below. Homogeneity prevailed through most of March and April in the upper 350 m at station 319. The time series of potential temperatures at 60, 347, and 1345 m for the winter period show phases in late February to early March, where they agree to better than 0.2°C, but that correspondence is not necessarily equivalent with deep convection, because the intermediate depth temperature maximum might still have existed. Unfortunately, the 807-m instrument (Figure 2*a*) failed, which might have recorded this intermediate maximum.

At station 250 the temperature gradient across the 78- to 258-m range of the thermistor string was 0.5°C in summer and increased to >1°C during November to January, interrupted by phases of very weak gradients (Figure 4*b*). Near-surface cooling to <−1°C similar to its occurrence at station 319 was not observed at and below the top sensor level of 78 m until February, and slow vertical penetration of cooling continued into late April, due to the continuing presence of the ice (is odden, Figure 1*b*) in this region. Homogeneity over the measurement range of the thermistor string was never observed during the winter period at station 250 because influx of fresher polar water by the Jan Mayen Current provided increased stability at that station compared to those in the central Greenland Sea.

At station T6 the temperature record from the ADCP temperature sensor in 200-m depth cooled down to −1.5°C (Figure 4*c*) during late January similar to station 319 (Figure 4*a*). After a brief warmer period, that depth range appeared to be part of the mixed layer during late February to mid-March. At station T5 the temperatures, again recorded there by the ADCP, show much larger variations than at either T6 or 319. Even in winter, when the 141-m temperature dropped to below −1.5°C, warmer periods of days to

weeks were observed with temperatures near 0°C. These fluctuations indicate that T5 was situated near the polar front, separating the warmer East Greenland Current from the colder central Greenland Sea.

Deep potential temperatures for stations 250, 319, and T6 show variations between −1.05 and −1.25°C (Figure 4*d*). The period of minimum deep temperature variance was December to February when ice was present over the region. In early to mid-March, sporadic deep temperature drops of up to 0.15°C occurred at the central Greenland Sea stations 319 and T6, that appeared to be related to deep convection, as discussed later. Consequently, temperature variability at station T6 has a maximum in late winter and spring, decaying into summer, while at stations 319 and 250, remnant variability from the preceding season lasts even into summer and fall.

Much of the temperature variability may be caused by horizontal advection of the fairly small-scale eddies of the region. Inertial-internal wave noise cannot be a large fraction of this variability, since at a mean vertical temperature gradient of only 0.1°C/300 m at 1400-m depth, a significant contribution would require large amplitudes for which other evidence does not exist. Spatial variability at the 1400-m level among four CTD casts taken by the R/V *Meteor* in the Greenland Sea in November 1988 was about 0.1°C, i.e., of the same magnitude as the observed variability. The baroclinic Rossby radius for intermediate depths was determined at 8–10 km. It seems that water mass inhomogeneities trapped in such eddies and advected by the fixed-point measurements make the bulk of the observed variability, while eddy "doming" would again require unrealistically large isopycnal and isotherm excursions to explain it. Reduced variability during the period of ice coverage consequently would be a combination of decay of water mass contrasts from the past winter through diffusion, of low level of advection and low energy of the higher-frequency motions during this time period.

In late winter, when the moored temperature data showed homogeneity to at least 350 m, shipboard hydrographic work in the central Greenland Sea was carried out by the *Valdivia* and *Hakon Mosby*. *Hakon Mosby* did a hydrographic survey with a towed fish undulating between 20 and 250 m with sections passing by our stations T5, T6, and 319 on March 13 and 14, 1989 [*Johannessen and Sandven*, 1989; O. M. Johannessen, personal communication, 1991]. At that time the ice edge was just west of station T5, while T6 and 319 were well within the ice-free area. A section of that survey running meridionally past T6 shows (within the contouring intervals of 0.1°C and 0.01 psu) homogeneous water of about −1.4°C and 34.87 psu several tens of kilometers to the north and south of T6 on March 14; and a section passing about 10 km east of 319 showed a change from stratified to unstratified near station 319. In fact, our near-surface temperature records of station 319 began to show a recurrence of upper layer stratification around March 8 (Figure 4*a*). When sections approached the ice edge, near-surface salinities and temperatures both decreased, which also was the situation on March 13 near T5.

A deep station taken during the *Hakon Mosby* survey only 7 km east of station T6 early on March 16, however, showed a steady downward temperature increase below 300 m, resulting in the 1300- to 2000-m level being 0.4°C warmer than the near-surface layer; this was accompanied by a salinity increase of approximately 0.03 psu over that depth range, resulting in an overall weak stability of the water column. The survey of *Johannessen and Sandven* [1989] had several other deep stations in the ice-free zone in the vicinity of the array, but all of them showed stable but weak deep stratification. A CTD cast taken by *Valdivia* 25 km southwest of station T6 on March 9 showed homogeneity to about 1400 m [*GSP Group*, 1990; *Rhein*, 1991], but at two other stations in the vicinity, only the upper few hundred meters were homogeneous.

In summary, the early March hydrographic surveys showed that a patch of >50 km extent existed, centered at about 75°N, 2°W, where the water was near-homogeneous, to at least 250 m (the maximum sensor depth), as result of mixed-layer deepening in the first half of February; but that homogeneity to greater depths occurred only sporadically and was of small horizontal extent.

4. Moored Current Observations

Horizontal Currents

Annual means and standard deviations of the horizontal currents measured by ADCPs and rotor current meters at stations 250, 319, T5, and T6 are given in Table 1. The low magnitude of these mean values came as a surprise to us. While the weak southward near-surface currents at 319 are in agreement with cyclonic circulation around the Greenland Sea (Figure 1*a*), the westward mean at station T5 and the southwestward flow at station 250 are not. But longer time series are required to establish stable means at this small magnitude of the circulation.

The time series of the 40-hour low-passed horizontal currents (Figure 5) are dominated by mesoscale current variations in the weeks-to-months period range with amplitudes generally less than 10 cm s^{-1} and eddy kinetic energies over the year-long deployment period of 35–75 cm^2 s^{-2} in the upper 300 m (Table 1). Figure 5*a* shows the ADCP currents at station 319 for different depths between 76 and 320 m together with Aanderaa current meter records from 347 and 1345 m. Two facts are obvious, independent of the so far unexplained ACM/ADCP speed difference discussed earlier. First, the currents were generally fairly barotropic and, second, the amplitudes were drastically reduced in the central Greenland Sea in December to January during the period of firm ice coverage, as indicated in Figure 5*a*. The amplitude reduction causes the rotor of the ACMs to stall during most of this time period, as during other weak current periods. Eddy kinetic energies during the period of ice cover in the central Greenland Sea are typically less than half the annual values (Table 1). One conclusion might be that this significant amplitude reduction of currents under the ice could suggest the primary energy source for deep current variations during the ice-free period to be wind forcing, but it could also be reduced instability generation of eddies by the larger scale flow. This matter needs further investigation.

The ADCP currents from the 230-m level at the four stations T5, T6, 319, and 250 (Figure 5*b*) indicate that the horizontal correlation scale of these currents is small compared to station separations. For the horizontal comparison, one has to keep in mind that the ADCP compass correction in T6, 319, and 250 may have left residual errors and that no correction could be applied to the T5 current directions.

TABLE 1. Current Statistics of Year-Long GSP Mooring Deployments

Station	Position	Deployment Time	Water Depth, m	Record Depth, m	Deployment Mean, cm s^{-1}		Fluctuating Kinetic Energy, cm^2 s^{-2}		
					East	North	Year	1.12–20.1	25.1–20.3
319 ADCP	74°57′N, 40°59′W	17.06.88–28.05.89	3554	76	0.0 ± 7.6	−3.2 ± 6.7	51	30	46
				161	0.3 ± 7.1	−2.8 ± 6.2	45	17	35
				231	0.3 ± 6.8	−2.7 ± 6.0	40	16	30
				320	0.3 ± 6.5	−2.6 ± 5.7	37	15	26
319 ACMs				347	0.1 ± 3.9	−1.4 ± 3.6	14	4	4
				1345	0.5 ± 3.5	−1.7 ± 3.4	12	4	2
T6 ADCP	75°03′N, 2°58′W	22.09.88–20.08.89	3624	231	0.3 ± 6.5	−0.2 ± 6.4	37	17	33
				320	0.3 ± 6.2	−0.1 ± 6.3	37	15	30
				452	0.2 ± 6.0	−0.0 ± 6.1	36	13	23
				1150	0.5 ± 5.2	0.1 ± 5.4	27	11	12
				1368	0.5 ± 5.0	0.0 ± 5.2	26	11	10
T5 ADCP	75°34′N, 6°07′W	14.09.88–30.08.89	3374	161	−1.9 ± 6.7	−0.4 ± 6.7	51	34	44
				231	−1.8 ± 6.5	−0.2 ± 6.4	42	31	41
				320	−1.7 ± 6.0	0.0 ± 6.0	36	23	35
				452	−1.5 ± 5.9	0.2 ± 5.8	34	20	32
250 ADCP	73°21′N, 0°48′W	20.09.88–20.08.89	3008	76	−0.9 ± 8.9	−2.3 ± 8.4	75	17	182
				161	−1.0 ± 6.5	−1.7 ± 6.1	40	12	37
				231	−1.0 ± 6.0	−1.6 ± 5.8	69	20	51
				320	−0.9 ± 5.6	−1.5 ± 5.5	30	10	18
250 ACMs				371	0.2 ± 3.9	−0.2 ± 4.0	15	5	9
				825	0.5 ± 2.5	0.2 ± 2.5	6	3	7
				1437	0.7 ± 1.8	0.5 ± 1.8	3	2	5

The mid-depth velocities of station T6 (Figure 5*c*) resemble those of the upper level (Figure 5*b*), underscoring again the dominantly barotropic nature of the mesoscale currents in the center of the Greenland Sea Gyre throughout the year. At station 250, located at the rim of the Greenland Sea dome (Figures 1 and 5*c*), the middepth currents were much weaker than in the center of the gyre, were more baroclinic, and had a more extended minimum during the winter season, paralleling the extended presence of ice over that is odden position (Figures 5*b* and 5*c*).

The shorter period variance in the upper 350 m was dominated by inertial period motions that were related to the passage of storms and probably also the location of the MIZ. Maximum energy in this period band occurred in the shallow mixed layer under the ice. At the 1000- to 1400-m level, station T6L, only one significant event of inertial period energy was observed and that was related to the mid-February storm and mixed-layer deepening, discussed below.

Vertical Currents

A time series of unfiltered vertical velocity data from September 1988 to March 1989 from 160-m depth at station 319 (Figure 6) shows the different aspects that need to be considered. First, there was a mean bias in the velocities, which was always negative and had to do with the internal ADCP data processing. As a first approximation, to correct it, we will deduct the annual mean in the following. Second, there was a fairly pronounced diurnal cycle, particularly obvious below the surface mixed layer in September–October but also occurring in February–March, which was due to the vertical migration of zooplankton scatterers [*Fischer and Visbeck*, 1993]. While the mean diurnal cycle was about 1 cm s^{-1}, peaks exceeding ±2 cm s^{-1} can be associated with it. Third, there were short-period fluctuations of larger amplitudes than the diurnal cycle, e.g., during November 17–23 or February 14–16 (Figure 6). These are the velocity variations we are interested in within the context of this study and on which we will focus in the following.

As previously observed (SL91), high-frequency (HF) variance of the vertical velocity in homogeneous water, $\overline{w'^2}$, is a good indicator of convection activity in progress. In a summary picture for all five ADCPs, Figure 7 shows the 6-hour high-passed variance for selected depth bins of each instrument over the entire year of observations. Also marked is the occurrence of ice over the stations, determined from the different ice indicators as discussed in section 2. Some of the results of this figure are as follows.

1. None of the instruments shows significant HF vertical velocity variance in the time period May–September, indicating that vertical velocity variations not caused by surface buoyancy forcing are small.

2. Of the two near-surface and upward looking ADCPs, station 319, located in the central Greenland Sea, showed repeated events down to 320 m, while station 250, located at the rim of the cyclonic dome (Figure 1*a*), only shows activity fairly close to the surface.

3. During the period of firmly established ice coverage, late November to late January (Figure 1*b*), vertical velocity variance is minimal.

4. Increased occurrence of vertical velocity events is observed during the period of late January to March, when a bay of ice-free water has opened in the central Greenland Sea.

5. An association of vertical velocity events with the passage of the ice edge over a station cannot be construed.

6. At the deep ADCP of station T6, depth range 1100–1400 m, only small $\overline{w'^2}$ is observed.

7. Overall, and compared to the velocity variance in the

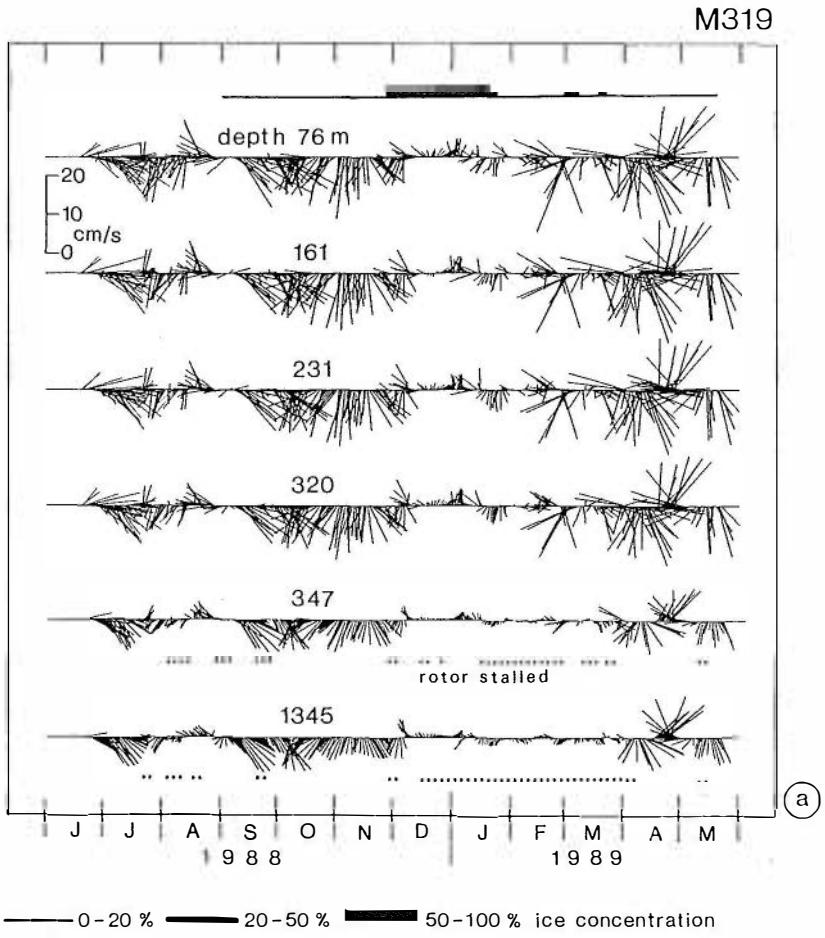

Fig. 5. (*a*) The 40-hour low-passed vector plots of horizontal ADCP currents (upward is northward) for several depths between 76 and 320 m at station 319, and for rotor currents at 347-m and 1345-m depths. Nominal speed of 2 cm s^{-1} is applied at time periods when rotors stalled (dotted). Ice coverage indicated by bar graphs. (*b*) The 40-hour low-passed vector plots of horizontal ADCP currents of stations T5, T6, 319, and 250 at depth level around 230 m. Ice coverage indicated by bar graphs. (*c*) Same as Figure 5*b* but for ADCP currents of stations T6 and rotor currents of stations 319 and 250 in depth range 1345–1437 m. Nominal speed of 2 cm s^{-1} is applied at time periods when rotors stalled (dotted).

300- to 600-m depth range of the Medoc area, which averaged $\overline{10}$ cm^2 s^{-2} over the time period of a week (SL91), the $\overline{w'^2}$ values of the Greenland Sea, in the winter of 1988–1989, were small (<2 cm^2 s^{-2}) below the near-surface layer.

Inspection of the individual vertical velocity time series has shown that, different from the findings of SL91 within a convective patch in the Mediterranean, individual downward events could occur in the Greenland Sea which would be averaged down to below the level of recognition in the 6-hour variance display of Figure 7. Therefore we also present, for the time period of likely convection, namely, late January when the ice edge recedes first back southwestward over some of the stations, to mid-March, time series of vertical velocities from two depths of each of the ADCPs (Figure 8*a*). Especially noteworthy are two short-period downward events of the deepest record, T6L, on March 6 and on March 16, which will be inspected more closely below. For comparison, the ECMWF heat flux components and wind stress are plotted on the same time scale as the vertical currents (Figure 8*b*).

5. Vertical Velocity Events

Mixed Layer and Thermocline Variability in October–November

A first event of vertical velocity variance at station 319 occurred in early October (Figure 7), simultaneously with the first cooling event (>400 W m^{-2}) in the ECMWF heat flux data. The pronounced variance peak in November (Figure 7) occurred in conjunction with a burst of northerly winds and the second similarly strong cooling event of the season. In October–November the mixed layer at station 319 was still quite shallow (<60-m depth, Figure 4*a*), and hence the velocity fluctuations observed in the depth range 160–320 m (Figure 7) occurred in stratified water.

The vertical velocity fluctuations of these first two events are symmetrical upward and downward motions (Figure 6), different from those observed during February and March, when the viewing range of the ADCP at station 319 was in homogeneous water. Consistency tests applied to the spectra and cross spectra of the vertical and horizontal currents show that these fluctuations were indeed internal waves.

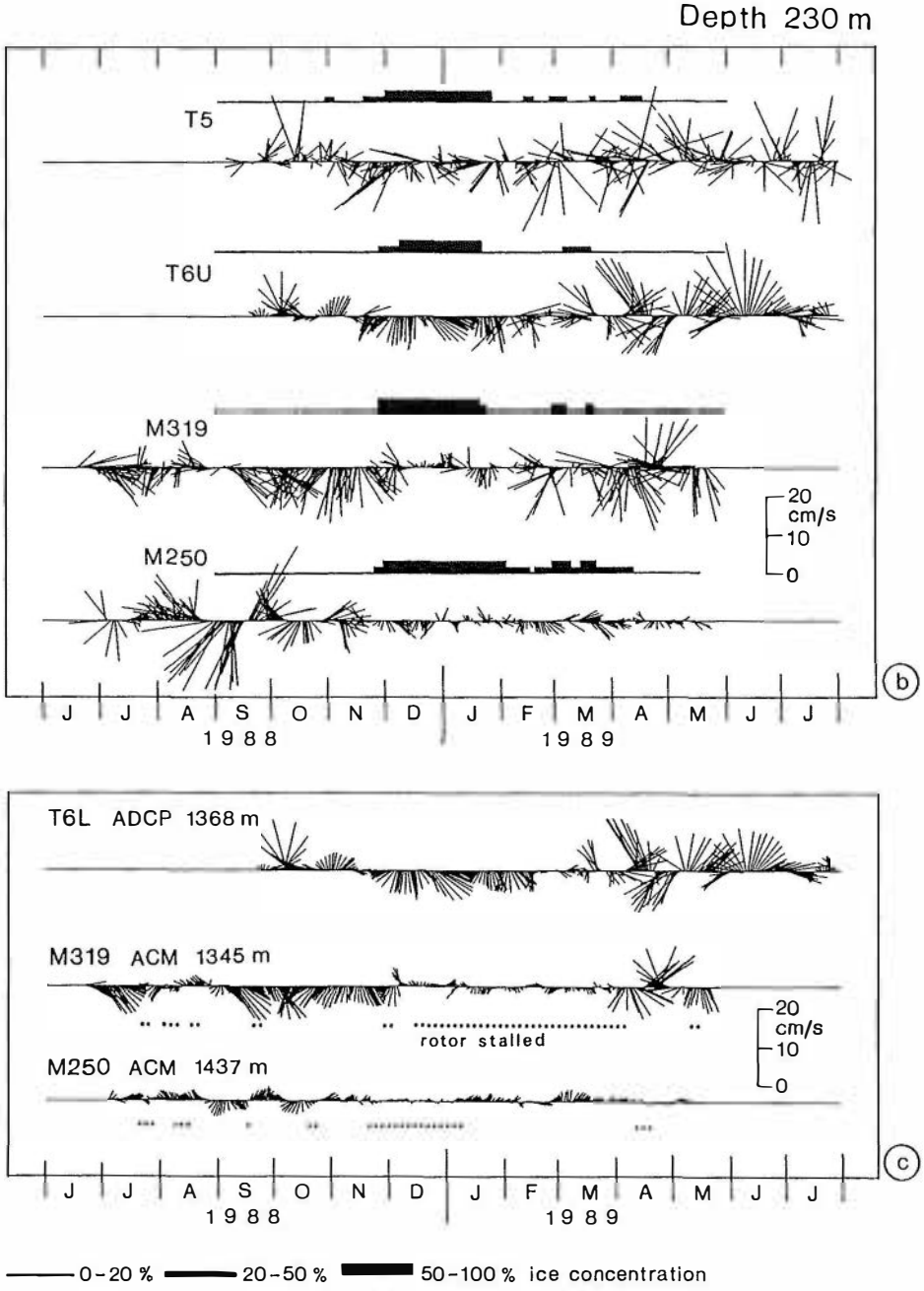

Fig. 5. (continued)

Their probable cause is convection activity in the shallow mixed layer, where cooled fluid parcels "bounce" on the stratified water masses beneath and generate internal waves. Against the late winter convection events these fluctuations are also distinguishable by a larger horizontal correlation scale, which is evident from the small error velocity variance, indicative of only small inconsistencies among the beam Doppler velocities (Figure 9).

Mixed-Layer Deepening in February

After the firm ice coverage over stations 319 and T6 ended on about January 23–25, two phases of progressive mixed-layer deepening were observed which caused the most significant changes in the upper layer temperatures observed during the entire winter period 1988–1989 (Figure 4*c*). The first phase is related to two southward wind bursts on January 27–28 and February 1–2, which were accompanied by heat losses of >500 W m^{-2} in the ECMWF data (Figure 8*b*). The second, stronger wind burst of the two was coupled with significant vertical velocity variance recorded by the ADCPs at stations 319, T5, and T6U (Figures 7 and 8*a*) and with mixed-layer deepening documented by the thermistor string at station 319 (Figures 4*a* and 8*c*) that lead to a homogenization down to at least 240 m. Simultaneously, the temperature of the mixed layer increased by 0.2°C to −1.4°C (Figure 8*c*). Entrainment velocity can be estimated from the vertical advancement of the mixed-layer depth past the thermistor chain sensors and results at about 0.3 cm s^{-1} for the 2-hour period of fastest vertical advancement. Vertical velocity variance for February 1 was 2.5 cm^2 s^{-2}, and error

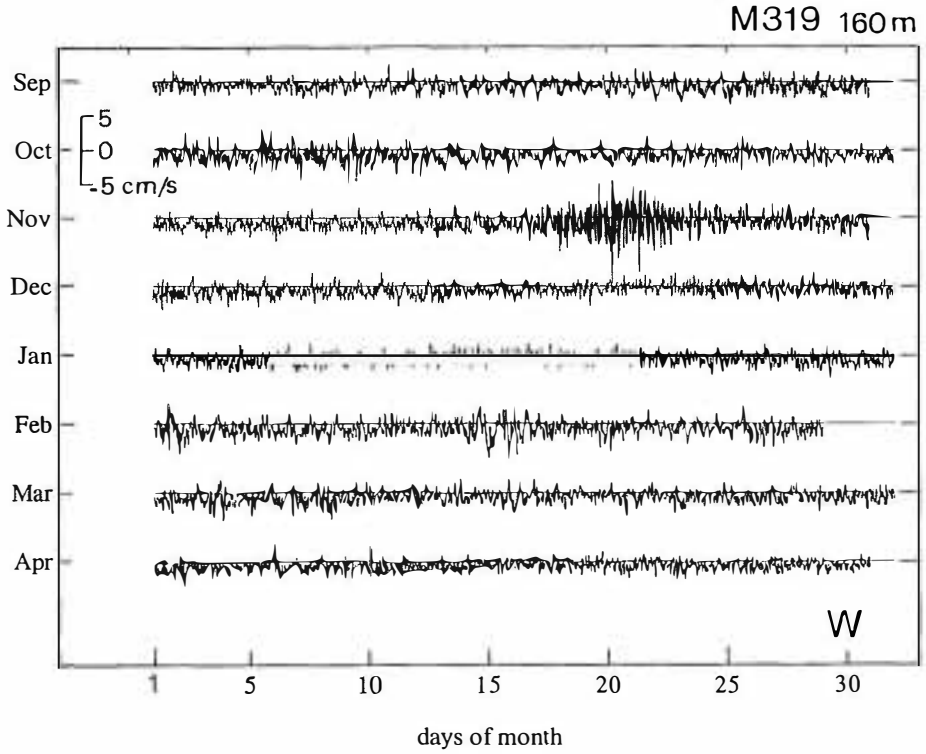

Fig. 6. Time series of half-hourly vertical ADCP currents during October 1, 1988, to April 30, 1989, from station 319 at 160-m depth.

velocity in the homogeneous water above about the 200-m level was larger than the vertical velocity accuracy, indicating small horizontal scale of the convection elements (Figure 9). This initial phase of mixed-layer deepening was also identified by *Guest and Davidson* [1991] as favorable for convection due to strong cold winds blowing from over the ice.

The second phase of this progressive mixed-layer deepening was associated with the southward wind burst and related heat loss maximum of 700 W m^{-2} during February 14–16 (Figure 8*b*). At this time the mixed-layer deepening reached the ACM temperature sensor at 345-m depth (Figure 8*c*). As a result of the further upward entrainment of warm intermediate layer water, the mixed layer temperature increased again by 0.1°C (Figure 8*c*). Vertical velocity variance and error velocity variance profiles were of the same magnitude at 200- to 250-m range (Figure 9), indicating similarly small horizontal scales as the February 1 event.

For both events the vertical mean velocity was not significantly different from the negative bias velocity. Furthermore, a relation between mixed-layer deepening and particular downward velocity events could not be established. In conclusion, the vertical velocity fluctuations of early and mid-February were apparently associated with three-dimensional mixed-layer turbulence due to the combined effects of wind mixing and cooling that caused deepening of the mixed-layer and entrainment of warmer waters from below. With wind stress as high as 1 N m^{-2} during these events (Figure 8*b*), the Ekman scale depth results as $uf^{-1} \sim$ 200 m, confirming that this phase was dominated by mixed-layer physics, not plume physics. The result was the large patch of homogeneous near-surface water in the central Greenland Sea that was subsequently observed by the *Hakon Mosby* Seasoar sections. This relatively shallow pool of mixed water was the source of subsequent convection to intermediate depths that was observed in the first half of March.

Individual Deep Events of March 6 and 16

Downward velocity events exceeding 3 cm s^{-1} were recorded by the deep ADCP T6L on March 6 and 16, as detectable in Figure 8*a* and shown on an expanded scale for March 2–20 in Figure 10*a*. The temperature recorded by the ADCP at 1400-m depth showed significant temperature decreases at the times when these downward events occurred (Figure 10*b*). These temperature decreases were, however, apparently not associated with total homogenization because the temperature at 200-m depth stayed about 0.1°C colder during and after the events (this difference is larger than the calibration error). At station 319, periods of deep temperature decreases similar to those at station T6 were recorded by the 1345-m ACM on March 6 and March 8–9 (Figure 10*d*).

A contour plot of the vertical velocities in the 1100- to 1370-m depth range at T6L for March 16 (Figure 11*b*) shows maximum downward velocities of 2.5 cm s^{-1} at 1100 m that increase to 3.5 cm s^{-1} at 1370 m at 1400 GMT. The downward velocity burst occurs simultaneously with the temperature decrease at 1400 m (Figure 11*a*). At the upper ADCP, in the 200- to 500-m depth range, the vertical currents (corrected for the mean diurnal plankton cycle) show strong (up to 3 cm s^{-1}) upward motion above 300 m early on March 16 (Figure 11*b*) and weak downward motion at 1000–1200 GMT occurring later at 500 m than at 300 m. If this upper downward event were connected to the deep event occurring at around 1400 UT, this would mean a

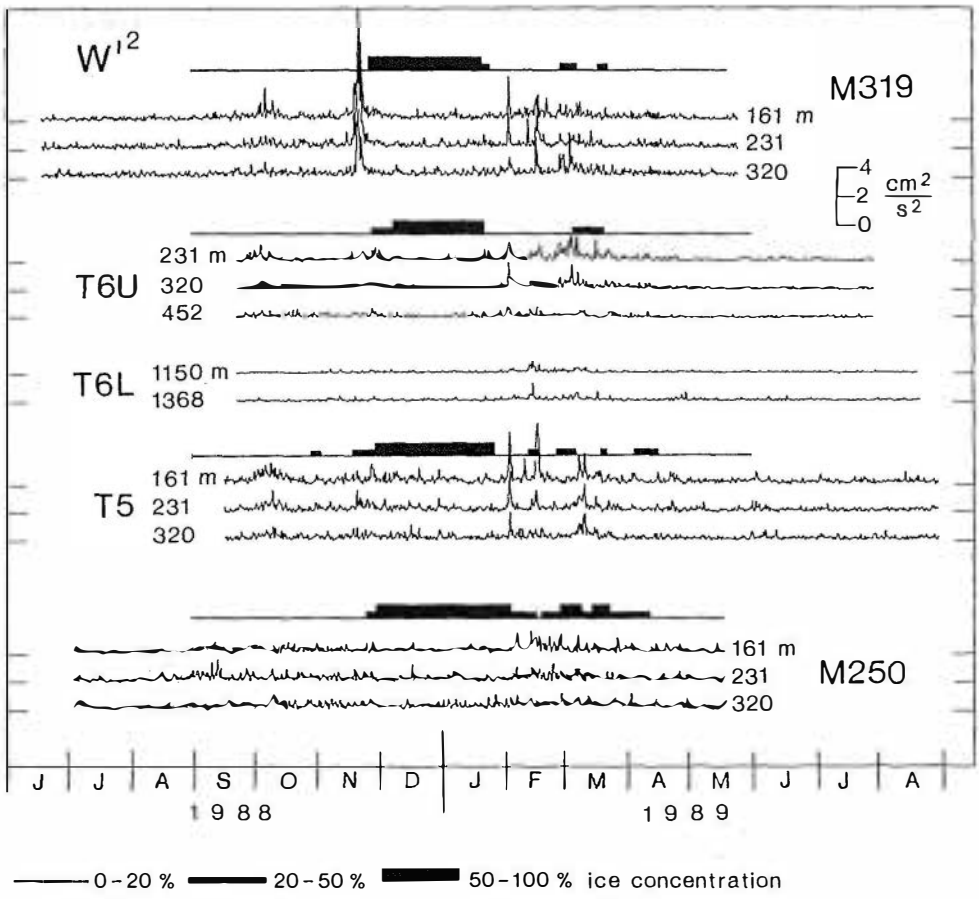

Fig. 7. Band-passed (periods >6 and <2 hours eliminated) variance of vertical velocity for several depths of each of the five ADCPs. Ice coverage indicated by bar graphs.

downward propagation of about 6 cm s^{-1} of the event from one ADCP to the other. The phase shift observed over the range of T6L alone was roughly one time interval of 1 hour at the upper bins compared to the lower bins, i.e., over 300 m, which would correspond to 8 cm s^{-1}, not too different from above estimate. This advancement speed of the plume is greater than the vertical velocity of 2–5 cm s^{-1} observed within the plume itself. One would expect, however, that the downward velocity within a plume should be at least about the same as the advancement speed of the bottom of it. The explanation is that the plumes are slanted when encountering the mooring.

If we estimate the horizontal scale of the deep plume from its encounter time of about 2 hours and advection speed of about 5 cm s^{-1}, it will be about 350 m. For a plume of this scale it would only take a vertical shear of the horizontal advection of 1 cm s^{-1} over 1000 m over the duration of about half a day to make the top of the plume sit sideways from its bottom. The result of such shear is an apparent phase shift of plumes as they encounter a vertical array of sensors. Horizontal currents prior to the event were westward and stronger at the 300- to 400-m level than at the 1200- to 1400-m level (Figure 11*c*), in support of this explanation.

There is also indication of horizontal circulation associated with this plume (Figure 11*c*): in the upper layer, T6U currents changed from the general westward flow to southwestward with the arrival of the plume at 1000–1100 GMT, which corresponds to cyclonic motion. In the deep layer, T6L currents changed from weakly westward to northwestward at 1100–1300 GMT, which corresponds to anticyclonic motion. The reverse vector rotations to be expected on the backside of the plume are not as obvious, however.

Plume temperature does not obtain at 1400-m depth the pool temperature of the 200-m level, for which entrainment of surrounding water during the descent may be responsible. Another possibility could be that water is not drained from the near-surface pool but from an intermediate layer below, but there is no other evidence supporting this alternative.

On March 6 at 1800–2200 GMT there was another deep downward event (Figures 10*a* and 12*b*) which occurred simultaneously over the range 1100–1400 m and was accompanied by downward motion at T6U, in the 230- to 550-m depth range, where it was followed by even stronger upward motion immediately afterward. The decrease of temperature, however, at the 1400-m level begins at noon on March 6 (Figure 9*b*) with a short-period precursor as early as March 5 (Figure 10*b*) and is not as obviously coupled to vertical velocity events as the March 16 case. The advection at the time of the March 6 event is weak and variable (Figure 12), which may be why this event does not show as clear a plume cut as the March 16 event that is carried past the ADCP mooring by consistent westward flow.

Deep temperature variations, similar to those just reviewed for station T6, also occurred 60 km westward at station 319 on March 6 and 8 (Figure 10*d*). On March 6, homogeneity was observed at all sensors within the mea-

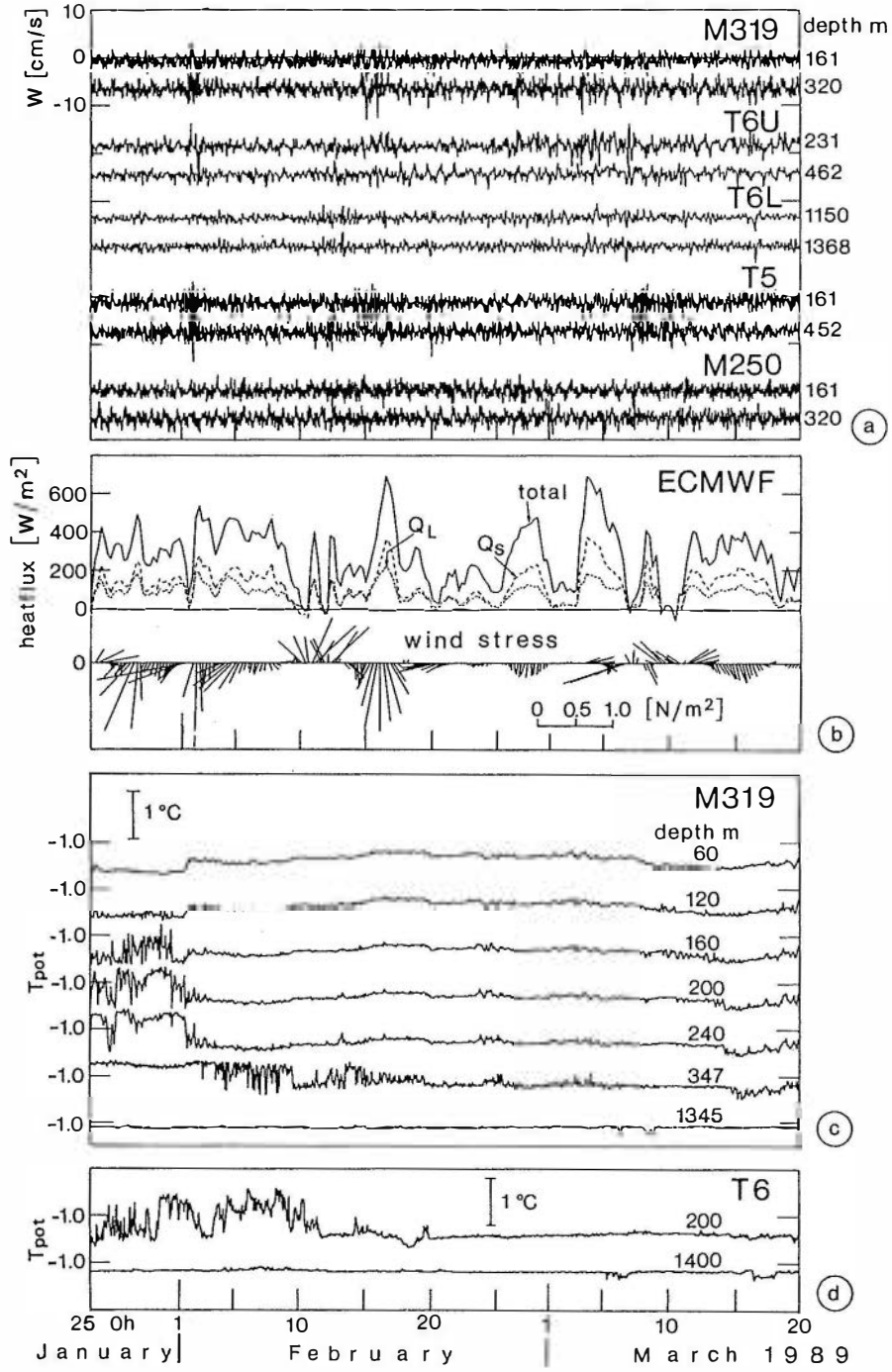

Fig. 8. (*a*) Vertical currents during January 25 to March 18 for two depths of each ADCP. (*b*) Sensible (Q_S), latent (Q_L), and total heat fluxes and wind stress from ECMWF model over central Greenland Sea. (*c*) Potential temperatures at station 319, from selected depths of thermistor string records and from ACMs at 347- and 1345-m depth; temperature offset between records is 1.0°C. (*d*) Potential temperatures from ADCPs of station T6 at 200- and 1400-m depth.

surement accuracy, while on March 8 the near-surface layer was restratified. This suggests that the latter event was due to advection of a plume that was convected elsewhere in the region.

It is noteworthy that the time scales of the deep temperature fluctuations are generally longer than the deep downward events (Figure 10*d*): they range from a few hours (March 6, station 319) to almost the two days of the cooling event initialized by the March 16 plume. This could mean that water spreads out of plumes horizontally into the upper part of the deep stratified layer and reaches larger horizontal extent there, in agreement with recent rotating tank experiments in stratified fluid (T. Maxworthy, personal communication, 1992).

6. Summary and Conclusions

During the winter of 1988–1989, five acoustic Doppler current profilers were moored at four positions in the Greenland Sea to measure vertical currents which might occur in

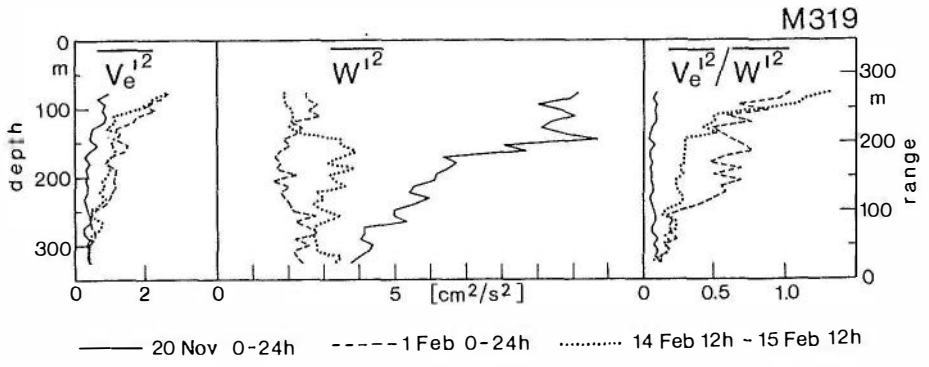

Fig. 9. Profiles of vertical ADCP velocity variance $\overline{w'^2}$, error velocity variance $\overline{v_e'^2}$ and of their ratio at station 319 for different 24-hour periods.

conjunction with deep mixing and convection. While four ADCPs recorded upper layer currents, one deep instrument recorded profiles in the depth range 1100–1400 m. From a technical viewpoint it was interesting that the backscatter of that deep instrument had the same range as found for the near-surface layer. Thermistor strings recorded upper layer temperature stratification at two of the positions, and deep temperature records were obtained at three stations.

The MIZ expanded eastward over the central Greenland Sea in late November and reached its maximum extent in late December. Under the ice a thin mixed layer with temperatures near the freezing point developed that gradually deepened during the ice cover period from 60 to 120 m. As simultaneously observed by *Roach et al.* [1993], brine rejection increased the salinity in the mixed layer, reducing stability against the stratified layer underneath and thus preconditioning the upper layer for subsequent mixed-layer deepening. Under the ice, convection activity below the mixed layer was not observed, and horizontal currents were significantly reduced with eddy kinetic energy less than half the annual value.

Beginning mid-January, a bay of ice-free water opened in the central Greenland Sea, around which a wedge of ice (the is-odden), almost 600 km long, curled around from the southwest, which existed throughout February and March (Figure 1*b*). The cause of this bay opening is not well understood as yet.

Spells of cold and dry wind blowing from the north via the ice over the ice-free bay, accompanied by heat losses of >500 W m^{-2} (according to ECMWF model output) caused surface-layer mixing and entrainment of waters from below. This occurred in two phases: the first around February 1 with mixed-layer deepening to 240 m and an entrainment velocity of up to 0.3 cm s^{-1}, determined for the time period of fastest vertical advancement of the bottom of the mixed layer past the thermistor string. The second phase occurred during February 14–16, when the mixed layer deepened to >347 m, the maximum sensor depth of our central Greenland Sea mooring.

Both cooling and deepening periods were documented by vertical velocity variance maxima in the mixed layer, which was of small horizontal scale, less than about 200 m based on the Doppler beam inconsistencies. The February cooling occurred similarly at stations T6 and 319 in the central Greenland Sea, about 60 km apart, and Norwegian Seasoar surveys in March 1989 [*Johannessen and Sandven*, 1989] showed that this cooling had generated a large patch of >50 km extent of homogeneous water (down to the maximum Seasor depth of 250 m). This patch served as the preconditioning area for deep convection that was observed in early to mid-March: a homogeneous body of water resides over a weakly stratified sublayer, and not much additional buoyancy flux is needed for deep convection to occur. An important fact here is that deep convection was observed in March when ice was apparently not in the area; hence brine rejection by freezing as proposed by *Rudels* [1990] was most likely not a requirement for its occurrence. (It can, however, not be excluded with certainty that new ice was formed at the time of convective activity which was not detected by SSM/I.)

Deep temperature fluctuations were recorded on March 6 and 16 at station T6 in 1400-m depth and on March 6 and 8, 60 km to the west, at station 319. The March 16 event occurred in conjunction with downward motion of 3–5 cm s^{-1} recorded by ADCPs, both in the 1100- to 1400-m and the 200- to 500-m depth range. This event could be interpreted as a plume advected westward by a baroclinic mean current which caused the top of the plume to be detected earlier at the mooring than the bottom. Horizontal rotation associated with it appeared to be cyclonic at the upper levels and anticyclonic at depth. For the March 6 event, similarly strong deep downward velocities were observed, but due to small and variable advection, that event was not as well documented by the fixed-point profiles as the March 16 event.

What would be the relation between scales and heat flux for the deep-reaching convection events in March? If the event of March 16 would have been caused by a total heat flux Q_Σ = 400 W m^{-2} including a contribution of evaporation, Q_v = 200 W m^{-2} (Figure 8*b*), the surface buoyancy flux would be

$$B_0 = \frac{g\alpha Q_\Sigma}{\rho_0 c} + \frac{g\beta Q_v S}{\rho_0 L} \text{ m}^2 \text{ s}^{-3}$$

with α thermal and β haline expansion coefficients, S surface salinity, L evaporation heat, c specific heat, and ρ_0 density. Using $L = 2.5 \times 10^6$ J kg^{-1}, $c_p = 4.0 \times 10^3$ J kg^{-1} °C^{-1}, $\alpha = 3.6 \times 10^{-5}$ °C^{-1}, and $\beta = 7.8 \times 10^{-4}$ psu^{-1}, we obtain

$$B_0 = 3.4 \times 10^{-8} + 2.0 \times 10^{-8} \text{ m}^2 \text{ s}^{-3}$$

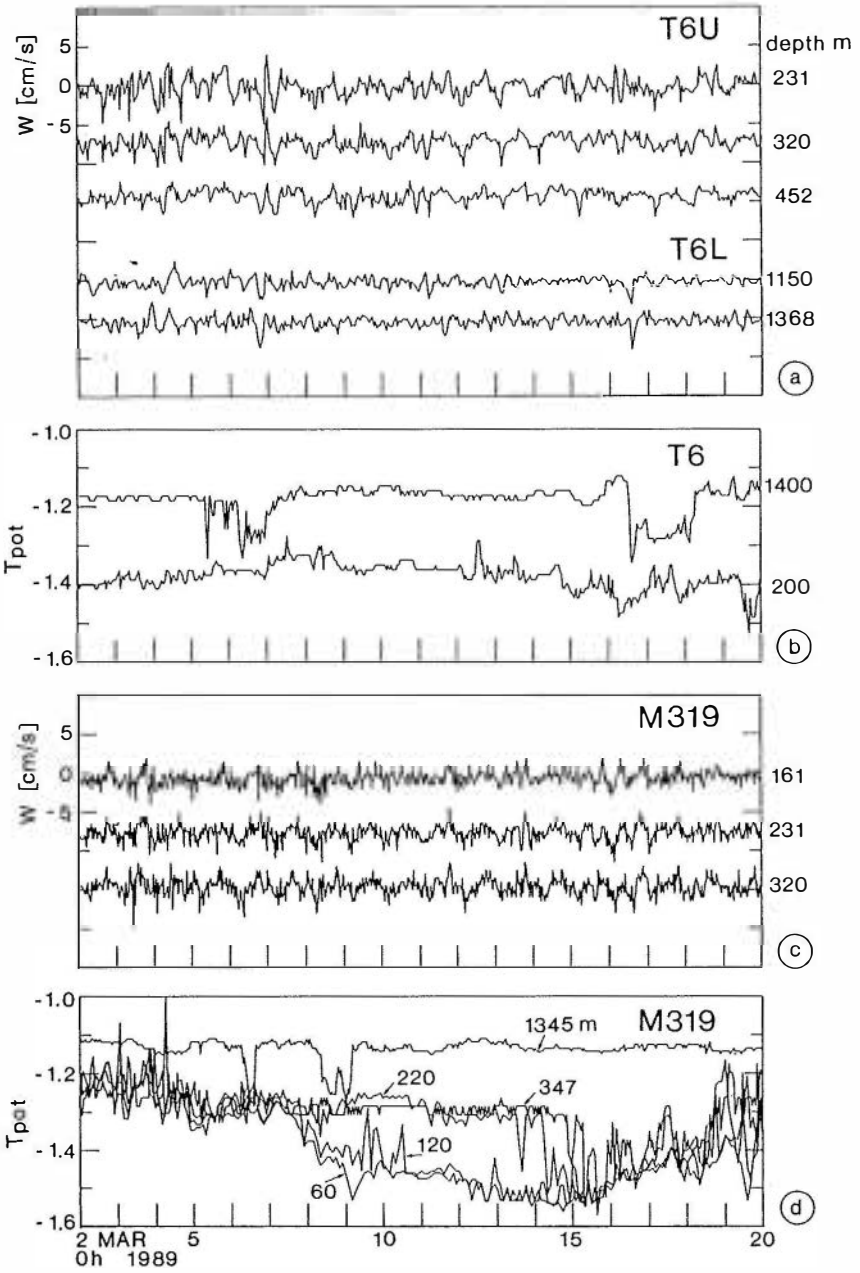

Fig. 10. (*a*) Vertical currents from several depths at position T6 during March 2–20. (*b*) Potential temperatures recorded by ADCPs at T6U in 200-m depth and at T6L in 1400-m depth. (*c*) Same as Figure 10*a* but for station 319. (*d*) Potential temperatures recorded at station 319 by thermistor string in 60-, 120-, and 220-m depth and by ACMs in 347- and 1345-m depth.

i.e., a substantial contribution comes from the haline flux, due to the low thermal expansion coefficient.

Assuming that the downward cooling events are caused by the surface buoyancy flux in the ice-free region, we can now relate the scales to be expected to the buoyancy flux, using the scaling arguments proposed by T. Maxworthy and S. Narimousa (personal communication, 1991) and advanced by *Jones and Marshall* [1993]. They are actually limited to neutral stability, but since deep stratification in the central Greenland Sea is very weak, this type of scaling should be acceptable.

The starting assumption there is that the potential energy increase caused by cooling and evaporation is transferred into kinetic energy of initial three-dimensional turbulence in a near-surface layer (the homogeneous preconditioning pool existing at that time in the central Greenland Sea). Upon further penetration of the convecting layer and on time scales approaching the inertial period, the Rossby number decreases to O(1), and rotation will affect the convection cells. At this stage, following these arguments, the essential scales of convection cells (plumes) will be only dependent on two outside parameters: surface buoyancy flux and rotation. The scale of the plumes will be approximately $l \sim (B_0/f^3)^{1/2}$, the density jump to surrounding water will be $g' \sim (B_0 f)^{1/2}$, and the velocity scale $w \sim (B_0/f)^{1/2}$. For our Greenland Sea case of $B_0 = 6 \times 10^{-8}$ m^2 s^{-3} and $f = 1.4 \times 10^{-4}$ s^{-1}, this yields $l \sim 220$ m, $w \sim 2.1$ cm s^{-1}, and $g' = 2.9 \times 10^{-6}$ m s^{-2}. The generation of rotating plumes in a cooling regime and the relevance of these scales was

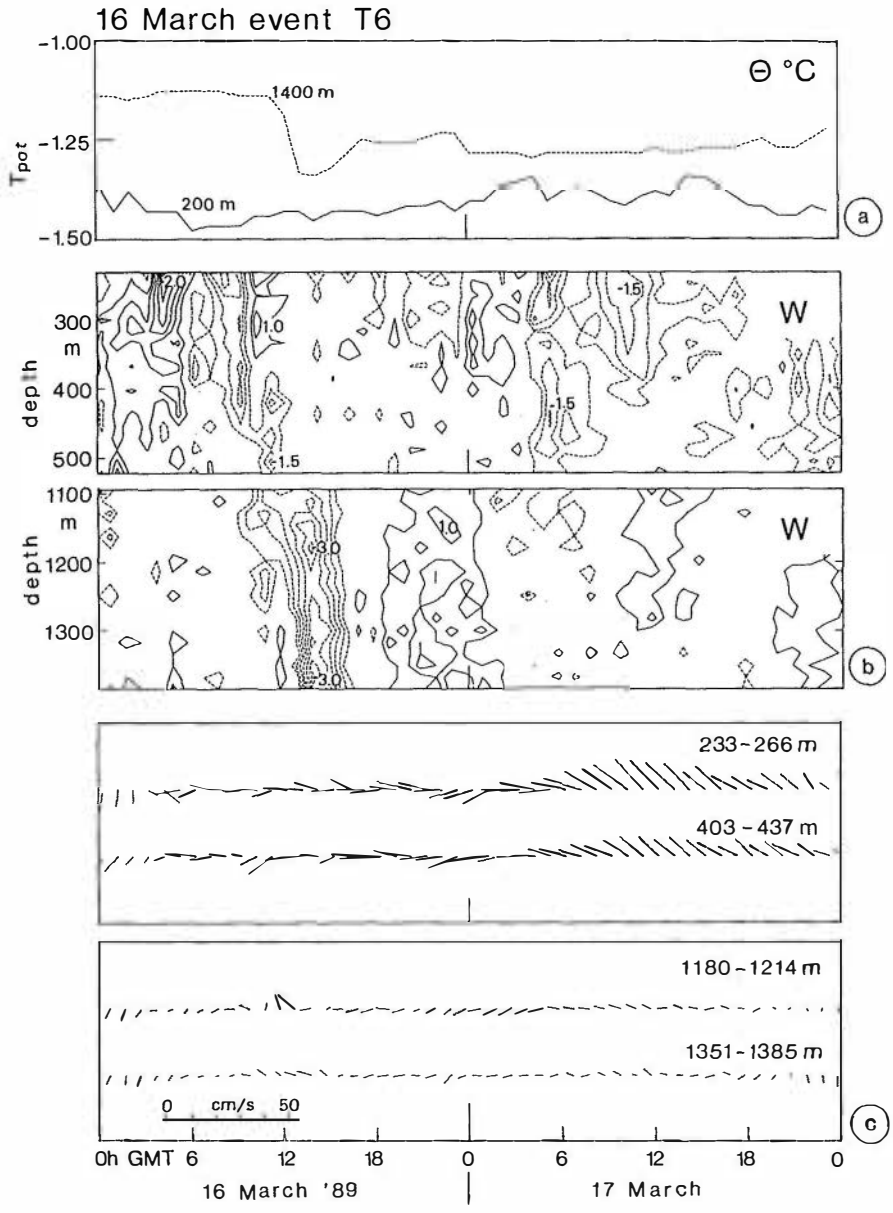

Fig. 11. Temperatures and currents at station T6 for the March 16 event. (*a*) Potential temperatures at 200-m and 1400-m depths. (*b*) Vertical velocity contour plot for depth ranges 250–510 m (T6U) and 1100–1368 m (T6L). Contour interval is 0.5 cm s^{-1}, upward velocity is contoured solid, downward is dashed, and zero contour is not drawn. (*c*) Horizontal current vectors in 233- to 266-m and 403- to 437-m depth range (T6U, top panel) and in 1180- to 1214-m and 1351- to 1385-m depth range (T6L, bottom panel).

shown by nonhydrostatic modeling [*Jones and Marshall*, 1993]. However, new similar numerical experiments in which the (isotropic) viscosity coefficient that was held constant in the above model experiment, was also varied, showed a dependence of plume scales also on the viscosity coefficient (J. Sander, personal communication, 1992).

Concerning the scale of the March 16 event, we can only estimate, from the passage time of about 2 hours and advection velocity of about 5 cm s^{-1} (Figure 11), that the horizontal scale should be about 350 m, i.e., of the same order as above scaling estimate. The observed velocity scale is also in agreement. The temperature jump of 0.15°C (Figure 10*b*), however, is much larger than the g' of the above cooling example would require; that would only be 0.01°C. As CTD casts (e.g., Figure 13) from the region showed, the fairly large temperature anomalies observed at intermediate depths (Figure 10) are almost compensated by salinity, yielding near-zero density fluctuations.

In summary, from our own observations and those of others, this experiment has shown the sequence leading to convection is started by brine rejection under the ice during late November to January that, together with mixed-layer temperatures near the freezing point of −1.9°C, causes minimum stability at the end of the ice cover period. Warmer, saltier water of Atlantic origin from deeper levels significantly contributes to the preconditioning. It does this either by direct entrainment and upward mixing or by upwelling caused by Ekman transport divergence related to

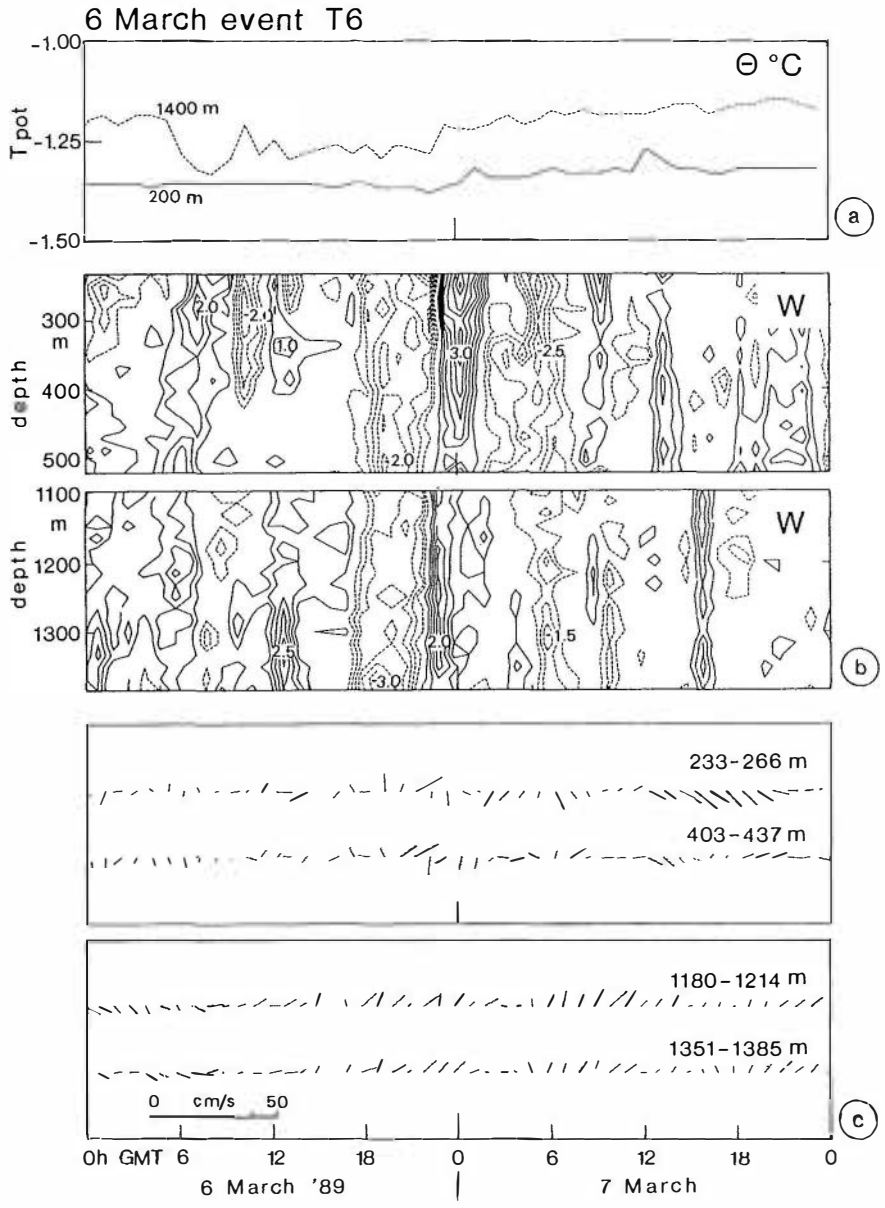

Fig. 12. Temperatures and currents at station T6 for the March 6 event. (*a*) Potential temperatures at 200-m and 1400-m depth. (*b*) Vertical velocity contour plot for depth ranges 250–510 m (T6U) and 1100–1368 m (T6L). Contour intervall is 0.5 cm s^{-1}, upward velocity is contoured solid, downward is dashed, and zero contour is not drawn. (*c*) Horizontal current vectors in 233- to 266-m and 403- to 437-m depth range (T6U) and in 1180- to 1214-m and 1351- to 1385-m depth range (T6L).

the partial presence of ice. We could not detect significant upwelling related to the passage of the MIZ in our temperature records. This second phase is dominated by mixed-layer physics, not plume physics.

This preconditioned pool of homogeneous water in the central Greenland Sea of >50 km extent permits the occurrence of convective plumes in March. Why they occur between March 6 and 16 is not obvious from our meteorological flux data; maybe the near-surface pool needed further salinization through evaporation (the salinization by evaporation during February corresponds to that of the formation of about 0.2 m ice), or by brief new ice formation events that were not detected by SSM/I. The current structure of at least one individual plume was observed by the ADCPs that extended down to the 1400-m level and seemed to match the scaling arguments put forward recently. Plume temperatures that were increased against that of the near-surface homogeneous pool suggested that warmer waters from intermediate layers were entrained on the way down. There were also indications that plumes "mushroomed" out into the stratification at intermediate depths. An interesting finding was that a mean downward motion during day-long periods of short-period convection activity were not distinguishable from zero. This result was different from the strong Mistral case investigated by SL91, where a 1 cm s^{-1} downward motion over the 1-week period of the Mistral cooling was determined. The Greenland Sea result suggests that plumes act like a mixing agent rather than carrying mean flow down-

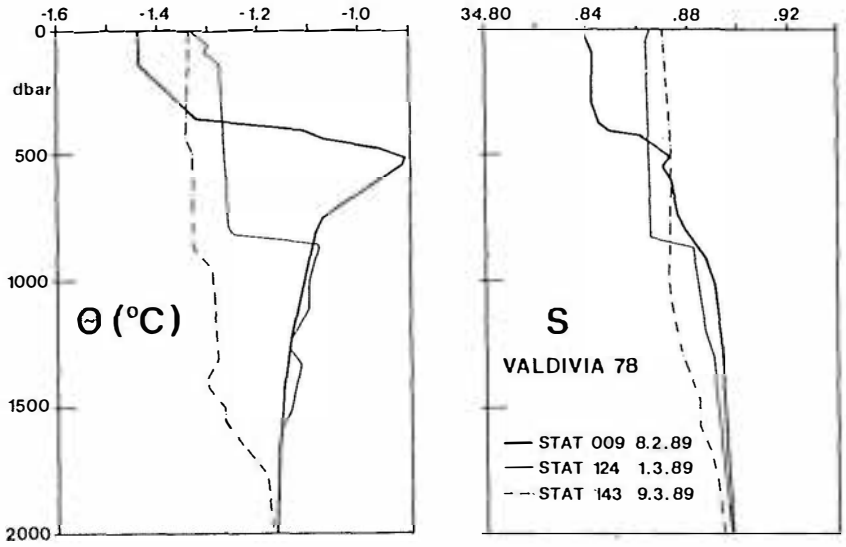

Fig. 13. Consecutive profiles of potential temperature θ and salinity S from the central Greenland Sea on February 8, March 1, and March 9, 1989 [from *GSP Group*, 1990].

ward. On the other hand, plumes did not fill up the entire volume above 1400 m, leaving large horizontal inhomogeneities in the convection region and causing only incomplete mixing.

Altogether, convective activity observed in winter 1988–1989 was weak compared with that recorded during a strong Mistral in the northwestern Mediterranean by SL91. Since tracer evidence requires [e.g., *Smethie et al.*, 1986] that convection at times must also go to the 3000-m level, this suggests that stronger convection activities than observed by us in winter 1988–1989 must occur, if sparsely.

Acknowledgments. We thank the captain and crew of the R/V *Polarstern* and J. Meincke (IfM Hamburg) for help in deployment and retrieval of stations 319 and 250; for stations T5 and T6, we thank J. Lynch (WHOI) and P. Worcester (Scripps) of the GSP tomography group for integrating our ADCPs into their stations. We appreciate the help of C. Meinke of IfM Kiel in preparation and deployment of the ADCPs, which all returned excellent data, and we thank A. Eisele for drafting the figures. Ice charts were kindly provided by the Norwegiske Meteorologiske Institut, Oslo, and we were given the opportunity to inspect unpublished SSM/I ice concentrations determined by L. Toudal, P. Gudmandsen (Technical University, Copenhagen) and A. Shuchman (Environmental Research Center, Ann Arbor). O. Johannessen (Nansen Remote Sensing Center, Bergen) and D. Quadfasel (IfM Hamburg) shared their hydrographic data, and K. Aagaard (NOAA/PMEL, Seattle) his moored station data from T6. We appreciate helpful comments of the anonymous reviewers that helped us to improve the manuscript. This study was supported by Bundesministerium für Forschung und Technologie (BMFT) under contract MFG 0071-8.

REFERENCES

Aagaard, K., J. H. Swift, and E. C. Carmack, Thermohaline circulation in the Arctic Mediterranean Seas, *J. Geophys. Res.*, *90*(C3), 4833–4846, 1985.

Belliveau, D., G. Bryden, and S. Melrose, Measuring ice motion—From below, *Sea Technol.*, *30*, 10–12, 1989.

Brugge, R., H. L. Jones, and J. C. Marshall, Non-hydrostatic ocean modelling for studies of open-ocean deep convection, in *Deep Convection and Deep Water Formation in the Oceans*, edited by P. C. Chu and J. C. Gascard, pp. 325–340, Elsevier, New York, 1991.

Carmack, E., and K. Aagaard, On the deep water of the Greenland Sea, *Deep Sea Res.*, *20*, 687–715, 1973.

Chereskin, T. K., E. Firing, and J. A. Gast, Identifying and screening filter skew and noise bias in acoustic Doppler current profiler measurements, *J. Atmos. Oceanic Technol.*, *6*, 1040–1054, 1989.

Clarke, R. A., and J.-C. Gascard, The formation of Labrador Sea water, I, Large-scale processes, *J. Phys. Oceanogr.*, *13*, 1764–1778, 1983.

Clarke, R. A., J. H. Swift, J. L. Reid, and K. P. Koltermann, The formation of Greenland Sea Deep Water: Double diffusion or deep convection?, *Deep Sea Res.*, *37*, 1385–1424, 1990.

Dietrich, G., Atlas of the hydrography of the northern North Atlantic Ocean, 140 pp., Serv. Hydrogr., Int. Council for the Explor. of the Sea, Copenhagen, 1969.

Fischer, J., and M. Visbeck, Seasonal variation of the daily zooplankton migration in the Greenland Sea, *Deep Sea Res.*, in press, 1993.

GSP Group, Greenland Sea project: A venture toward improved understanding of the ocean's role in climate, *Eos Trans. AGU*, *71*(24), 750–755, 1990.

Guest, P. S., and K. L. Davidson, Meteorological triggers for deep convection in the Greenland Sea, in *Deep Convection and Deep Water Formation in the Oceans*, edited by P. C. Chu and J. C. Gascard, pp. 369–375, Elsevier, New York, 1991.

Häkkinen, S., Upwelling at the ice edge: A mechanism for deep water formation?, *J. Geophys. Res.*, *92*(C5), 5031–5034, 1987.

Johannessen, O. M., and S. Sandven, SIZEX 89: A prelaunch ERS-1 experiment, *Tech. Rep. 23*, 39 pp., Nansen Remote Sens. Cent., Bergen, Norway, 1989.

Jones, H., and J. Marshall, Convection with rotation in a neutral ocean: A study of open-ocean deep convection, *J. Phys. Oceanogr.*, in press, 1993.

Koltermann, P., and H. Lüthje, Hydrographic atlas of the Greenland and northern Norwegian Seas (1979–1987), *Publ. 2328*, 274 pp., Deut. Hydrogr. Inst., Hamburg, 1989.

Lazier, J. R., The renewal of Labrador Sea water, *Deep Sea Res.*, *20*, 341–353, 1973.

Legutke, S., A numerical investigation of the circulation in the Greenland and Norwegian Seas, *J. Phys. Oceanogr.*, *21*, 118–148, 1991.

McDougall, T. J., Greenland Sea bottom water formation: A balance between advection and double-diffusion, *Deep Sea Res.*, *30*, 1109–1117, 1983.

MEDOC Group, Observation of formation of deep water in the Mediterranean Sea 1969, *Nature*, *227*, 1037–1040, 1970.

Mirbach, K. J., Windvektormessungen mit Akustik-Doppler-Profilmeßgeräten, Dipl. thesis, Univ. of Kiel, Germany, 1991.

Quadfasel, D., and J. Meincke, Note on the thermal structure of the Greenland Sea gyre, *Deep Sea Res.*, *34*, 1883–1888, 1987.

RD Instruments, Acoustic Doppler current profilers; principles of operation: A practical primer, 36 pp., San Diego, Calif., 1989.

Rhein, M., Ventilation rates of the Greenland and Norwegian seas derived from distributions of the chlorofluoromethanes F11 and F12, *Deep Sea Res.*, *38*(4), 485–503, 1991.

Roach, A. T., K. Aagaard, and F. Carsey, Coupled ice-ocean variability in the Greenland Sea, *Dyn. Atmos. Oceans*, in press, 1993.

Rudels, B., Haline convection in the Greenland Sea, *Deep Sea Res.*, *37*(9), 1491–1511, 1990.

Rudels, B., D. Quadfasel, H. Friedrich, and M.-N. Houssais, Greenland Sea convection in the winter of 1987–1988, *J. Geophys. Res.*, *94*(C3), 3223–3227, 1989.

Schott, F., Effects of a thermistor string mounted between the beams of an acoustic Doppler current profiler, *J. Atmos. Oceanic Technol.*, *5*, 154–159, 1988.

Schott, F., Measuring winds from underneath the ocean surface by upward looking acoustic Doppler current profilers, *J. Geophys. Res.*, *94*, 8313–8321, 1989.

Schott, F., and K. D. Leaman, Observations with moored acoustic Doppler current profilers in the convection regime in the Gulf of Lions, winter 1987, *J. Phys. Oceanogr.*, *21*, 558–574, 1991.

Smethie, W. M., Jr., H. G. Östlund, and H. H. Loosli, Ventilation of the deep Greenland and Norwegian seas: Evidence from krypton 85, tritium, carbon 14, and argon 39, *Deep Sea Res.*, *33*, 675–703, 1986.

van Aken, H. M., D. Quadfasel, and A. Warpakowski, The Arctic front in the Greenland Sea during February 1989: Hydrographic and biological observations, *J. Geophys. Res.*, *96*, 4739–4750, 1991.

Vinje, T. E., Sea ice conditions in the European sector of the marginal seas of the Arctic, 1966–75, *Arbok. Nor. Polarinst.*, *1975*, 163–174, 1977.

Worcester, P. F., B. D. Cornuelle, and R. C. Spindel, A review of ocean acoustic tomography: 1987–1990, *Rev. Geophys.*, *29*, *suppl.*, 557–570, 1991.

J. Fischer, F. Schott, and M. Visbeck, Institut für Meereskunde an der Universität Kiel, Dusternbrooker Weg 20, 24105 Kiel 1, Germany.

(Received April 17, 1992;
revised December 12, 1992;
accepted January 6, 1993.)